Journal Pre-proof

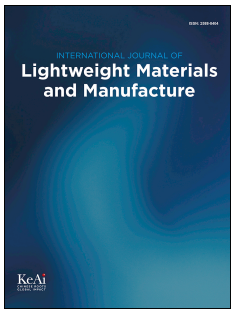

Design and fabrication of lightweight thin-shell structures using shape memory polymer composites for lunar habitat systems

Sandaruwan Jayalath, Uditha Roshan, Janitha Jeewantha, Jayantha Epaarachchi, Eduardo Trifoni, Madhubhashitha Herath, Eleftherios E. Gdoutos, Bandu Samarasekara

PII: S2588-8404(26)00003-X

DOI: https://doi.org/10.1016/j.ijlmm.2026.01.003

Reference: IJLMM 430

To appear in: *International Journal of Lightweight Materials and Manufacture*

Received Date: 18 November 2025

Revised Date: 9 December 2025

Accepted Date: 6 January 2026

Please cite this article as: S. Jayalath, U. Roshan, J. Jeewantha, J. Epaarachchi, E. Trifoni, M. Herath, E.E. Gdoutos, B. Samarasekara, Design and fabrication of lightweight thin-shell structures using shape memory polymer composites for lunar habitat systems, *International Journal of Lightweight Materials and Manufacture*, https://doi.org/10.1016/j.ijlmm.2026.01.003.

Design and fabrication of lightweight thin-shell structures using shape memory polymer composites for lunar habitat systems

Abstract

The increasing demand for lightweight, rigid, and deployable structures in space exploration has driven the development of advanced materials for lunar and orbital habitats. This study presents the design, fabrication, and validation of modular thin-shell components based on shape memory polymer composites (SMPCs) for deployable rigid habitats. Moreover, the durability in unexplored, harsh environmental conditions and the lower weight are the governing factors for these materials. In this context, well-developed and durable shape memory polymer-based composites (SMPCs) are ideal for these habitats due to their potential to create lightweight, thin-shell structures and their proven ability to revert to their original shape when stimulated by external factors, such as heat and light. Furthermore, this enables the manufacture of SMPC habitat components on Earth, allowing for reduced storage space in payloads, and facilitates the recovery and rebuilding of habitats after transportation. During this study Bisphenol-A cyanate ester based shape memory polymer was synthesised and reinforced with glass fibres and graphene nanoplatelets to achieve quasi-isotropic properties and enhanced thermal stability. Using vacuum-assisted resin infusion, hemispherical thin-shell modules (1 mm thickness) were manufactured and programmed into compact configurations for efficient payload storage. Experimental evaluation demonstrated excellent shape recovery (>95%) and adhesive joint strength, while distributed optical fibre sensing enabled precise strain mapping during programming and recovery. Finite element analysis validated the structural integrity of the assembled dome under internal pressures up to 2 atm, confirming its suitability for lunar habitat applications. Furthermore, this work can be considered one of the pioneering works to use space grade SMPCs in future lunar habitats. The proposed SMPC-based architecture offers a promising solution for lightweight, reconfigurable structures in future space missions, combining deployability, mechanical robustness, and thermal resilience.

Keywords: *Cyanate esters, deployable rigid structures, lunar habitats, shape memory polymer composites, space applications, thin-shell structures.*

1 Introduction

Pursuing sustainable lunar habitation is at the forefront of current aerospace engineering, as evidenced by NASA's timeline for establishing the Artemis Base Camp near the lunar South Pole by 2030. This endeavour is supported by insights from initiatives like the "3D-Printed Habitat Challenge," which ran from 2015 to 2019, aimed at pioneering habitat construction techniques applicable to both lunar and Martian environments. The burgeoning interest and research within global space industries emphasise two primary methodologies for constructing lunar habitats: inflatable (deployable) technologies and self-sustainable, 3D-printed rigid habitats that utilise lunar regolith as a primary resource [1,2]. An evaluation by Higgins. et al. in 2020 [2] highlight the potential advantages of inflatable habitat concepts over their rigid counterparts. It also suggests that hybrid models could offer even greater benefits. Therefore, the need for materials that exhibit both deployability and rigidity emerges as a critical factor in the design and development of these habitats. The transportation and assembly of heavy, large modules present notable challenges, especially on the Moon or in low Earth orbit. A potential solution lies in using lightweight materials, specifically polymer composites, which have been extensively studied for their favourable properties in such applications. Further alleviating transport concerns, the feasibility of folding or programming modular components to occupy minimal space within a rocket's payload fairing presents a promising avenue for innovation. Recent research conducted by Wang et al. in 2024 [3] reinforces this concept, indicating that incorporating a Shape Memory Polymer (SMP) rigidization layer into rigidizable inflatable multilayer structures can significantly enhance structural integrity and dynamic properties, thereby preventing collapse during deployment. Consequently, shape memory polymers and their composites emerge as exceptional candidates for future lunar habitat projects, offering a balance of resilience, adaptability, and lightweight characteristics. This paper will delve into the potential applications of these advanced materials and construction methods in creating effective and resilient habitats on the Moon, discussing the technological developments that pave the way for humanity's next steps in extraterrestrial colonisation.

Many different SMP and SMPC materials have been developed throughout the past decade, aiming for various components in space applications [4–8]. So far, most of them were deployable hinges [9], truss booms [10], switches and rollable tubes [11,12] with bending mechanisms. SMPCs are often fabricated with unidirectional or plain-weave fibres with orthotropic properties to facilitate this bending movement of the developed non-structural components. Due to that, this fibre lay-up configuration does not allow the composite to bear stresses in multiple in-plane directions. Therefore, SMPC development with quasi-isotropic properties (in-plane isotropic properties) for deployable load-bearing structures is a novel initiative in the field of SMPCs. The proportion of fibres oriented in a specific direction within the laminate can be calculated and referred to as the directional ply percentage.

The GTX SMPC developed by the leading author [13,14] is used in this research study. This SMPC was developed with 0/90° and ±45° plies as a sandwich lay-up architecture and acts as a quasi-isotropic sheet with at least 12.5% of directional ply percentage towards the main eight directions [15]. A well-developed and durable SMPC, such as GTX SMPC [16] in this category will allow the development of deployable structures such as reflector antennas, modular components, equipment chambers, morphing structures, deployable dwelling units, and space debris capture systems. The primary application of this study is the use of GTX SMPC in the development of deployable lunar habitat structures.

First, the authors detail manufacturing a thin-shell SMPC component, specifically an eighth of a hemispherical dome shape (Octant Hemispherical Section (OHS)) as shown in Figure 1(b1), for use in an individual dome Figure 1(b3) or in a hemispherical dish-ended pressure vessel shape Figure 1(b5). As shown in Figure 1, this component is expected to be manufactured on Earth, programmed into space-saving flattened shapes, transported to space or the lunar environment, and finally used as a part of modular habitat construction after recovering to its original shape. A vacuum-assisted resin infusion technique was used to manufacture the OHS. This is mainly due to the complex shape of the SMPC and the high-temperature handling of the uncured SMP mixture. As one of the main objectives of this research work, the shape memory behaviour of complex shapes was measured using a distributed optical fibre network (DOFN) [17,18] embedded inside the SMPC OHS. In-plane strain occurred due to the vertical deflection of the component, while shape memory programming was measured using an optical backscattered reflectometer. Finally, a finite element model of the OHS component and an assembled dome structure were analysed for their shape memory behaviour and structural integrity, respectively. The finite element models were validated with less than 5% error, creating a benchmark for future habitat developments.

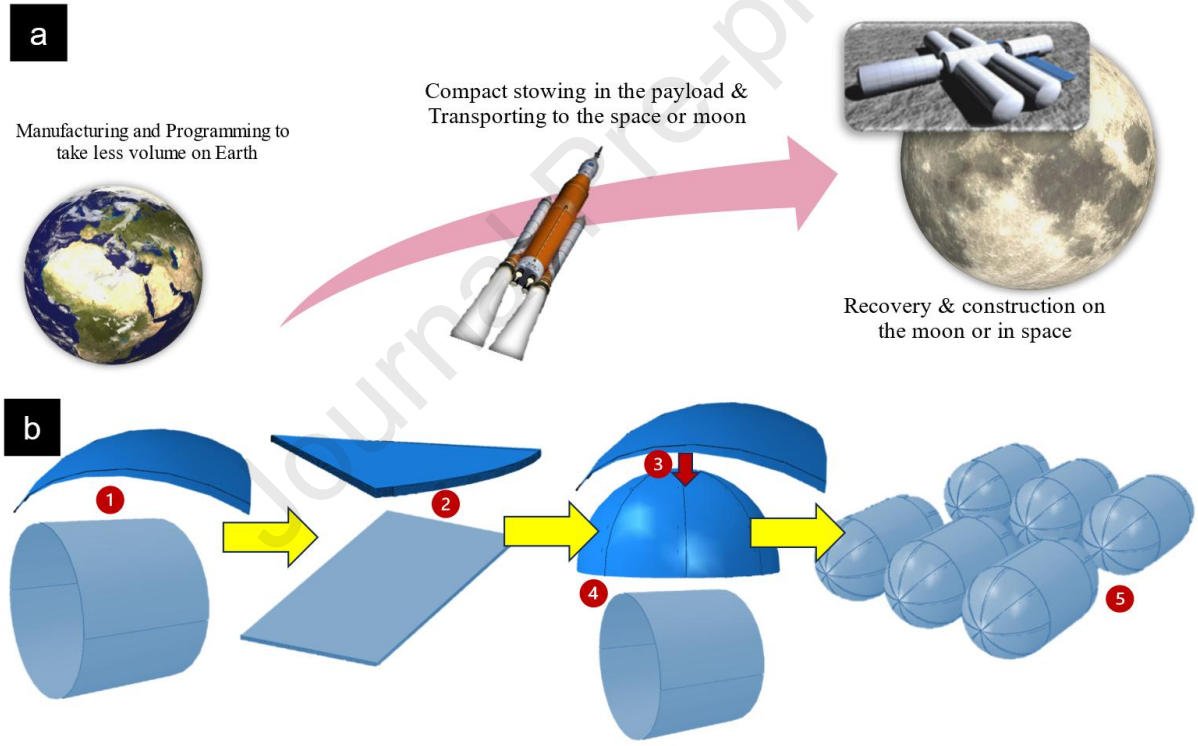

Figure 1: (a) 45° sectional SMPC component (OHS) manufacturing, transportation and assembly in space or on the moon. (b) SMPC component 1. In manufactured shape 2. Programmed, then stacked 3, recovered, then 4. Assembled, and finally, 5. Construct to make multiple pressure vessel structures for habitats.

2 Experimentation

2.1 Materials and specimen preparation

Two types of chemicals were used with stoichiometric ratio variations for the SMP synthesis. BACE (M_n = 278.31; solid powder form) was used with PEG (M_n = 600; liquid form) as the base matrix material for SMP. BACE and PEGs were supplied by Wenzhou Blue Dolphin New Material Co. Ltd., China, and ChemSupply Australia, respectively. For the SMPC fabrication, glass fibre (GF) fabrics (0/90° plane-weave, 200 g/m^2) were supplied by ATL Composites, Australia, and were used as reinforcing fibre layers. The complementary behaviour of GF towards the shape memory behaviour was the primary reason for selecting GF as the reinforcing fibre. Furthermore, the thermal stability, low thermal expansion, and resistance to radiation of SiO_2 are also considered

in this selection. Graphene Nanoplatelets (GNP, surface area: 750 m^2/g) supplied by Sigma-Aldrich Australia were used as the thermal filler material to increase the thermal conductivity of the SMP.

During the SMP sample preparation, the measured BACE was heated up to 100°C until it fully melted, and the measured PEGs were added to the mixture with a BACE: PEG-9:1 stoichiometric ratio. The mixture was mixed using a mechanical stirrer for 30 minutes, then degassed in a vacuum oven at 11.15 kPa at 100°C for another 30 minutes. Then, the chemical mixture was used to fabricate cured SMPC sheets for mechanical tests carried out in Jayalath et al. (2024) [16]. Fabrication and curing of SMPC OHS components were carried out as detailed in the following section.

2.2 Fabrication of the SMPC test specimens, modular components and thin-shell dome.

The initial design of the OHS was created using the 3D parametric modelling software (SOLIDWORKS 2022/23). The hemisphere consists of eight equal sectional components. Each component has a sector angle of 45°, and an additional 4° seam with 0.4 mm thickness was kept, combining each part to form a complete hemispherical section (Figure 2(a)). A gap of 0.2 mm was designed between the seams to apply the adhesive. After combining individual components, the final hemisphere has an outer radius of 187.5 mm (D=375 mm) and a thickness of 1 mm (Figure 2(b)).

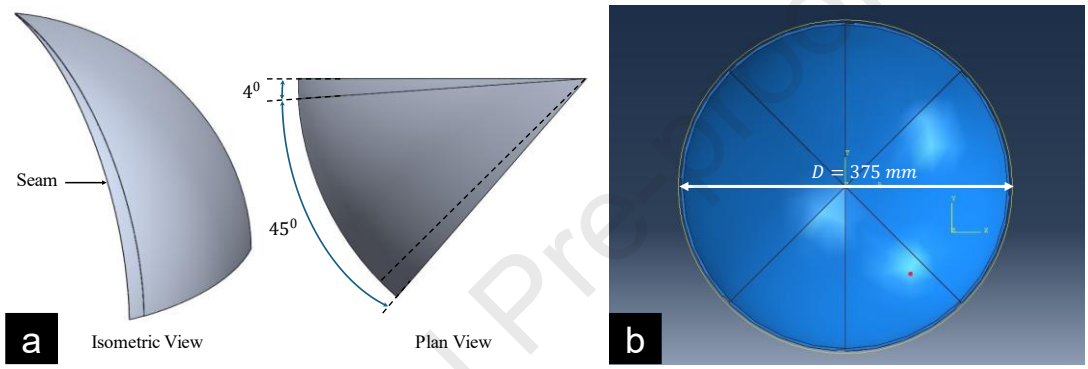

Figure 2: (a) Design of the octant hemispherical section (OHS) and (b) assembled hemispherical dome shape after combining 8 hemispherical components.

A mould (Figure 3) was designed utilising 3D parametric modelling software (SOLIDWORKS 2022-2023). The overall dimensions of the mould are 440 × 440 × 85 mm^3, with approximately 100 mm of clearance from the central cavity to the surface edges to accommodate the vacuum infusion apparatus. To optimise the design, material was selectively removed from non-critical areas to reduce the weight of the mould. Additionally, any sharp and steep corners of the component sections were smoothed out to ensure an even fibre lay-up, preventing issues like uneven thickness and wrinkles that could lead to misalignments during the assembly of the final hemispherical structure. The mould (Figure 4(a)) was manufactured by Kintec Machining Co., Ltd. in China, crafted from Aluminium (Al6061-T6 grade). A PTEF-coated glass fabric sticker, with a thickness of 0.25 mm and provided by Swift Supplies Pvt. Ltd. in Australia, was applied to the flat parts of the Aluminium mould (Figure 4(b)). This coating serves to inhibit the adhesion of the SMP mixture to the Aluminium surface during the curing process.

The SMPC components were fabricated using the vacuum-assisted moulding technique. High-temperature-resistant vacuum bagging tools and consumables supplied by Easy Composites Ltd, UK, were used due to higher curing temperatures over 180°C. First, a coupon was drawn using the projection curves of the 3D OHS using the "Flatten" feature in SOLIDWORKS software to accurately cut fibre layers (Figure 4(c & d)), which needed to be laid on top of the curved mould cavity. Then, the glass fibres with 0/90° and ±45° layups were cut using the coupon, as shown in Figure 4(c & d).

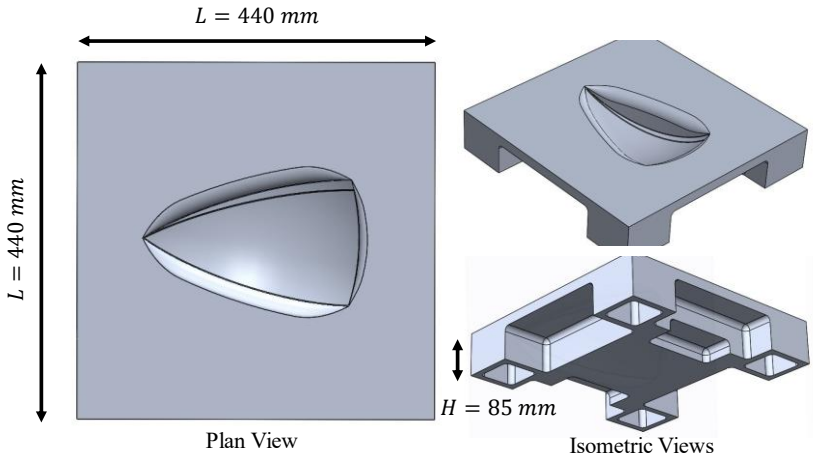

Figure 3: Plan and Isomeric views of the designed mould for the OHS fabrication.

During the fabrication process, a Teflon film was first laid on the mould. Then, six glass fibre layers were laid to get the TX fibre layup architecture. These six glass fibre layers with 0/90° and ±45° plane-weave configurations were laid alternatively as described in previous works of the leading author [13,16]. The pre-prepared SMP liquid mixture (at 90°C) was poured on the finished fibre layups, and the mixture was evenly spread using a fibreglass compression roller. Once the SMP mixture became solid at room temperature, the next 4 layers (peel-ply layer, infusion media, breather and vacuum bagging film) were laid subsequently (Figure 4(e), and the setup was vacuumed to achieve and seal the hemispherical component shape. Then, the whole setup was kept in the oven and left to cure for 3 hours at 100°C, 5 hours at 120°C, and 2 hours at 180°C. The partially-cured solid SMPC samples were then released from the vacuum infusion setup and post-cured at 210°C for another 5 hours. Finally, the excess parts of the SMPC OHS were cut using a mini handheld grinder to achieve the final shape Figure 5(a).

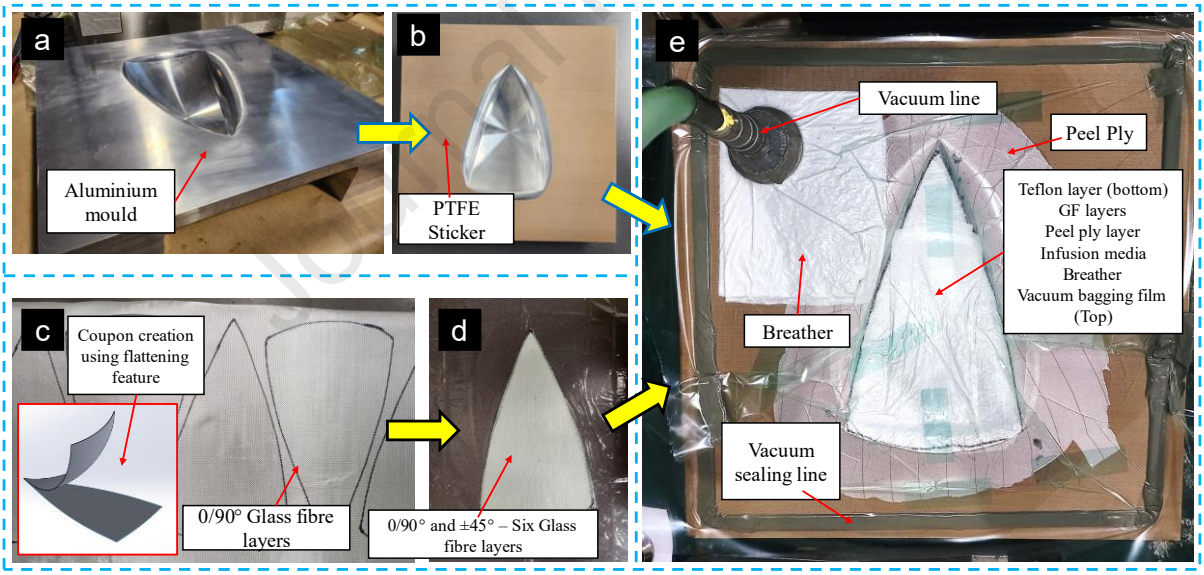

Figure 4: Steps of the OHS fabrication

The adhesive lap-shear joining method was used to join the hemispherical components together. Bisphenol A Cyanate Ester (BACE) pre-polymer supplied by Wenzhou Blue Dolphin New Material Co, Ltd, China. First, a BACE pre-polymer was applied to the seams of the OHSs (Figure 5(a)). Then, the seams are joined with overlap joints to get a hemispherical shape. All the joints were clamped, and the setup was cured for 5 hours at 120°C, 2 hours at 180°C and 5 hours at 210°C. Finally, the completed SMPC thin-shell hemispherical dome shape was achieved (Figure 5(c)).

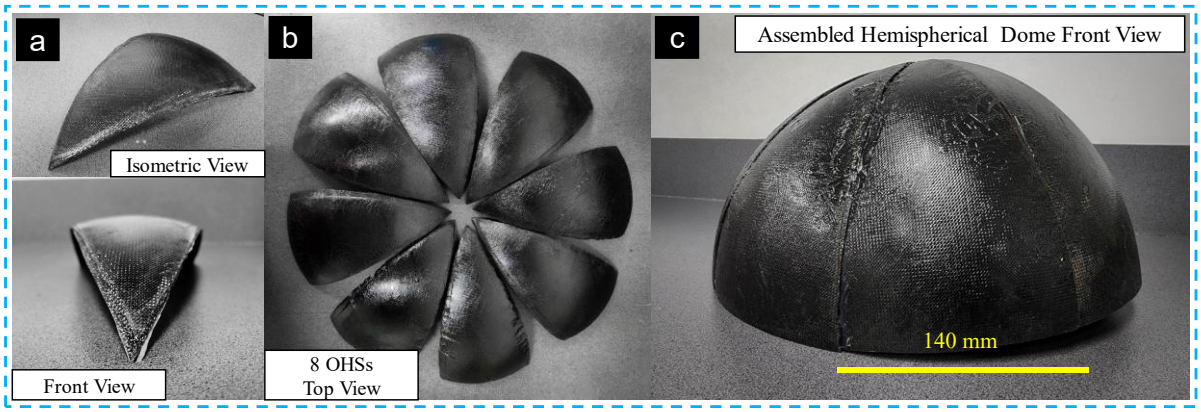

Figure 5: (a),(b) Fabricated SMPC OHS components and (c) the assembled hemispherical thin-shell dome.

2.3 Experimental property tests

2.3.1 Bond Strength Test

Measuring the bond strength of the adhesive-joined SMPC is important since the SMPC OHS was joined using the BACE pre-polymer adhesive. This joint can be a critically stressed area of the assembled hemispherical dome under air pressure. Therefore, the ASTM D5868 – 01 standard for single lap shear adhesive joints for fibre-reinforced plastics was followed to test the bond strength (Figure 6). First, overlapping areas of the SMPCs were roughened using 240 Grit sandpaper and the surface was cleaned using acetone. For this, two GTX SMPC samples with 25.4 mm × 101.6 mm were joined with an overlapping area of 25.4 × 25.4 mm^2. Cured samples were fixed in the MTS 100 kN uniaxial tensile testing machine using Aluminium tabs inside the fixtures to align the bond perfectly vertically. The loading rate was set to 13 mm/min according to the ASTM D5868 – 01 standard. The gathered data were used to validate the bond strength of the hemispherical thin-shell SMPC section.

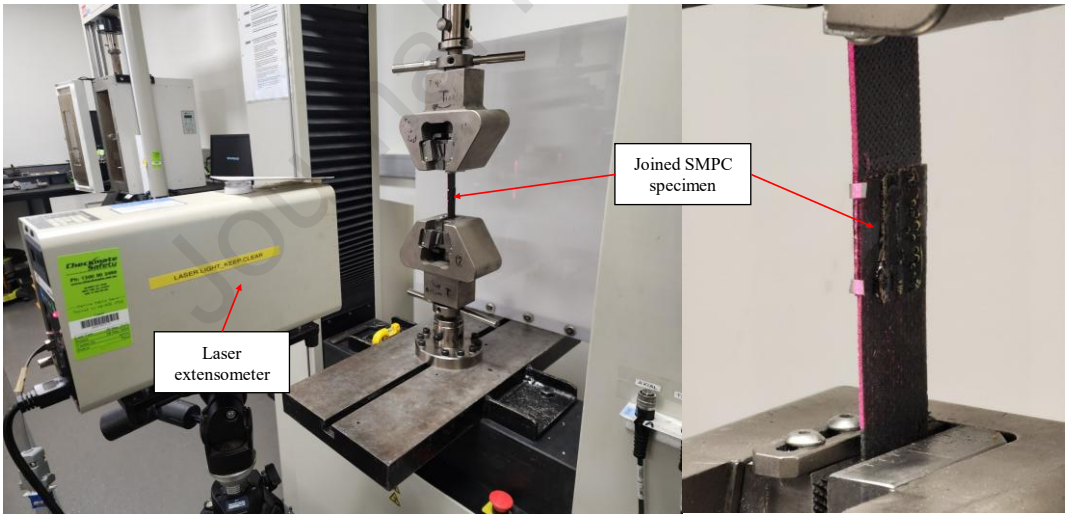

Figure 6: Bond strength test of the GTX SMPC.

2.3.2 Shape memory properties of the OHS modular components

Measuring the shape memory behaviour of complex shapes is a novel study in the field of SMPs. Depending on the shape, the measuring techniques can be changed, and custom made. As a complex 3D shape, the shape memory properties can be measured through the in-plane strains of the composite which is challenging. The authors developed a novel method addressing this, and it is discussed later in this section. Additionally, the shape memory properties can be measured considering the primary shape change of the SMPC component.

Since the SMPC OHS needs to be fully flattened to save space in a payload fairing, the vertically flattened shape (Figure 7) can be considered the 100% (vR_f) programmed shape. Therefore, initial shape programming of the OHS was done by keeping the components in an oven at 160°C for 30 min and then flattening them using a heat press until the maximum allowable shape. Then, the programmed shape was kept inside the vacuum oven (Labec, Australia) using clips on a wooden block to avoid heat transfer through conduction. Afterwards, the vacuum was

kept at 11.15 kPa (-89% vacuum), and the temperature increased to 160°C, allowing the OHS 30 min in the vacuum oven to be fully recovered. As shown in Figure 7 and equations 1 and 2, the vertical parametric equations developed were used to calculate the general shape programming and recovery ratios without damaging the OHS. Moreover, Equation 3 was developed to calculate the ideal shape fixity ratio (iR_f), considering the perfect shape fixation (when $d_1 = h_2$), where the component is fully flat.

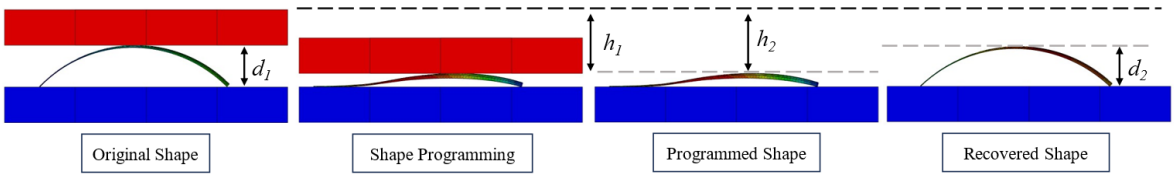

Figure 7: Vertical parametric method for the shape memory effect calculation.

$$vR_f = \frac{h_2}{h_1}100\% \qquad (1)$$

$$vR_r = \frac{d_2}{d_1}100\% \qquad (2)$$

$$iR_f = \frac{h_2}{d_1}100\% \qquad (3)$$

The main objective is to accurately measure the shape programming and recovery of complex SMPC shapes to use them in validating computer-aided models. An SMPC component was fabricated by embedding DOFN inside to address this. First, the 4th 0/90° fibre layer from the outside of the OHS was chosen to attach the optical fibre (Figure 8(a)). Then, the optical fibre (SMF 28 125 µm silica core/ single mode) was embedded in the glass fibre layer, and the component was fabricated, as shown in Figure 8. The optical fibre layout inside the component (Figure 9) was done to extract the strain from 11 designated points. Approximately 50 mm equal distances were kept between the optical fibre sensor lines. The length from the beginning to the 1st point in the sensor was measured as 67 mm. Further, the total distance of the optical fibre sensor was measured as 828 mm to the 11th point from the beginning of the sensor inside the SMPC OHS.

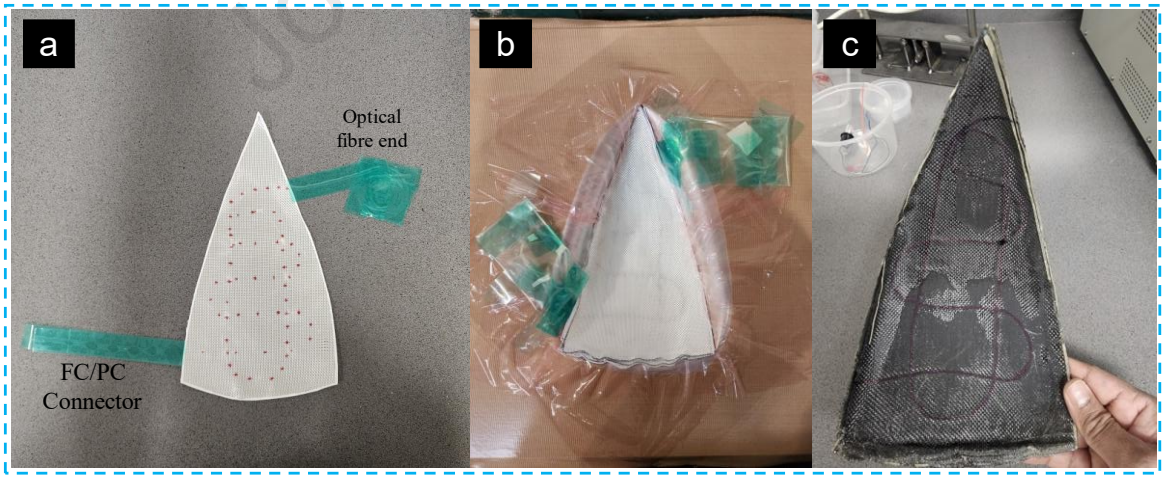

Figure 8: Optical fibre-embedding during the SMPC OHS fabrication process; (a) Knitted optical fibre through the 0/90° glass fibre layer, (b) complete fibre lay-ups on the mould including the layer with the optical fibre, and (c) finally cured OHS indicating the optical fibre path inside the component.

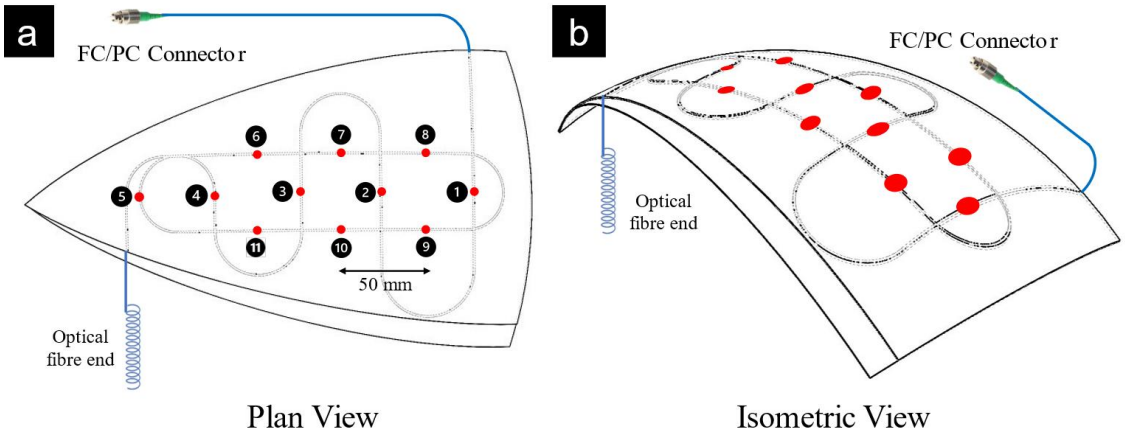

Figure 9: Optical fibre arrangement of the OHS component to measure in-plane strain changes during shape memory program and recovery.

During the testing process, the SMPC OHS was kept inside the environmental chamber of the MTS 10 kN tensile testing machine with the compression fixture/ head. The optical fibre was connected to the LUNA OBR 4600 (Optical Backscattered Reflectometer) using an FC/PC connector, and the strain measurements were taken using the static mode of the OBR 4600 (Figure 10) with a group index of 1.5, a spatial resolution of 0.1 mm and a 10 mm gauge length. The OHS was given vertical deflections using the compression head. Then, the strain and relevant force measurements were taken at different vertical deflections from 5, 10, 15, 20, and 25 mm at 120, 140, and 160°C. After the 25 mm vertical deflection at each temperature, the SMPC component was kept for 30 min in the programmed position and cooled down to room temperature. Static strain data from the OBR were acquired after each deflection. The readings were taken after maintaining the initial strain at zero at the beginning of each temperature to compensate for the increased strain of the optical fibre sensor due to thermal expansion. After each test, the SMPC OHS was allowed to recover at the tested temperatures. Finally, the gathered data was used to analyse the shape memory behaviour. The strain data gathered from the DOFN can be translated to study the in-plane tensile and compressive strain behaviour during shape memory programming and recovery of complex SMPC shapes. The measured strain in almost every direction provides the possibility to map the stresses in the areas of a complex shape where the fibre optic was embedded during the fabrication. It can further verify the FEA models of complex SMPC shapes.

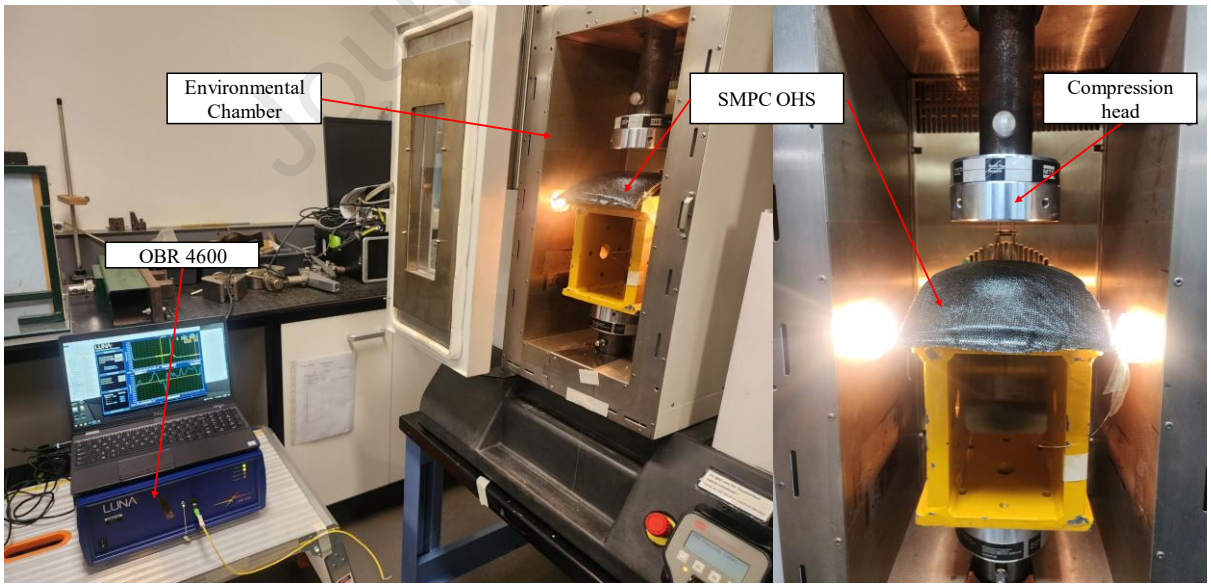

Figure 10: Experimental setup for measuring the strain under different deflection/loading conditions.

2.4 Finite element analysis specifications and used data

Validating the experimentally fabricated thin-shell components and dome structure using a finite element model can produce new knowledge to be used in similar structures. This allows the gathered knowledge to be used in future developments. Three finite element analyses were done addressing (1) the complex shape memory

programming process of the SMPC, (2) the adhesive single lap shear bond strength of the SMPC joint, and (3) the behaviour of the assembled thin-shell hemispherical dome under atmospheric pressure. ABAQUS CAE 2019 software package was used for this simulation. 3D modelling space was used for tasks (1) and (3), while 2D Planar modelling space was used for the (2) bond strength analysis. All the detailed descriptions of the elements in the simulations are listed in Table 1. For the modelling of a thin-shell hemispherical dome shape using finite element analysis (FEA), continuum-based shell elements were used. This is due to the capability of continuum shell elements to capture in-plane stress/ strain behaviour, which is crucial for composite materials [19]. The viscoelastic modelling for the shape memory behaviour was not specifically incorporated during this analysis as the authors has already verified the excellent shape programming and recovery behaviour during the SMPC development stage. Measuring the strain changes during shape programming, recovering and simulating the mechanical integrity of the hemispherical dome shape was the primary aim of using a DOFN.

Table 1: Detailed description of FEA model elements

	FEA Model Details of the SMPC and SMP Parts				
	(1) SMPC OHS Programming and Recovery Validation	**(2) Bond Strength Validation**		**(3) Thin-Shell Hemispherical Modular structure validation under air pressure**	
	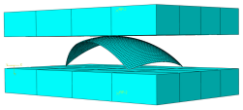			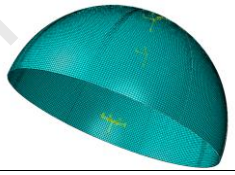	
Modelling Space	3D	2D Planer		3D	
Element Description:	**OHS Component:**	**GTX SMPC:**	**Adhesive Layer:**	**OHS Component:**	**Adhesive Layer:**
Element Library	Explicit	Standard	Standard	Explicit	Standard
Geometric Order	Linear	Linear	Linear	Linear	Linear
Family	Continuum Shell	Plane Stress	Cohesive	Continuum Shell	Cohesive
Element Shape	Hex	Quad	Quad	Hex	Wedge
Mesh Technique	Sweep	Free	Free	Sweep: for the component Structured: For the seams	Sweep
Mesh Size	4	0.5	0.5	3	5
Initial number of elements	5169	600	50	15909	221

Table 2: Material properties used in FEA simulations.

Specifications	**GTX**	**GT**	**GX**	**B9-N SMP/Adhesive**
Materials Behaviour	Elastic	Elastic	Elastic	Cohesive
Engineering Constants				
E1 (MPa)	7910 (4120 at 140°C)	9743.2	5327.3	1605
E2 (MPa)	7910 (4120 at 140°C)	9743.2	5327.3	
E3 (MPa)	3326.4	3326.4	3326.4	
v1	0.1771 (0.28 at 140°C)	0.0973	0.1931	0.1485
v2	0.1771	0.0973	0.1931	0.1485
v3	0.1485	0.1485	0.1485	0.1485
G1 (MPa)	3359.952	4439.795	2232.534	
G2 (MPa)	4138.646	4439.795	4083.123	
G3 (MPa)	1448.15	1448.15	1448.15	
Density (tonne/m^3)	1.472×10^{-9}	1.472×10^{-9}	1.472×10^{-9}	1.201×10^{-9}
Cohesive: Traction Separation				
Enn (MPa/mm)				8025
Ess/Ett (MPa/mm)				3494
Maxs Damage (Max Stress Damage Criteria)				
Nominal Stress – Normal (MPa)				66.2
Nominal Stress – First and Second Direction (MPa)				39.7
Damage Evolution -Fracture Energy (N/mm)				1.036

For the FEA, the GTX SMPC composite was assigned a composite layup architecture using the spherical coordinate system. Twelve repeating plies (0.083 mm thickness) with rotation angles of 0°, 90°, +45°, and -45° were added, and properties of GX and GT SMPCs were assigned to each layer (Figure A1 in Appendix). GTX

SMPC was considered a quasi-isotropic material in all directions of the lay-up plane. Properties of the B9-G SMP were used in the tangential direction of the SMPC. Elastic and cohesive properties [20–22] of the SMPCs and SMP were extracted and calculated from the gathered data in previous work by the lead author [13,14,16] and listed in Table 2. These data were used in the finite element analysis of this section.

3 Results and Discussion

3.1 Experimental Shape Memory Effect Evaluation

The initial height (d_1: as shown in Figure 7) of the OHS was measured as 64.04 mm. During the experimental programming of the SMPC OHS, an ideal vertical shape fixity (iR_f) of 43.65% was achieved with a maximum deflection (max h_2) of 27.24 mm with a general vertical shape fixity ratio (vR_f) of 100% and vertical shape recovery ratio (vR_r) of 99.4%, as shown in Figure 11. The spherical shape's inherent resistance to shape change can explain the lower shape fixity ability of the OHS [23,24].

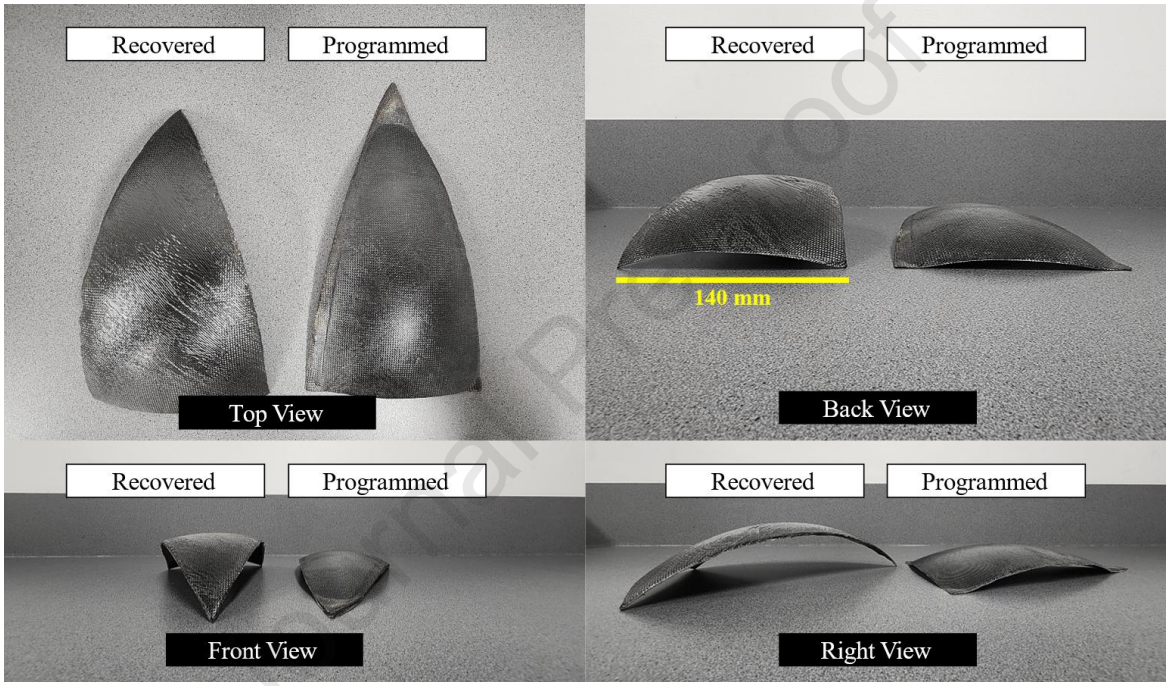

Figure 11: SMPC OHS with 100% R_r and 43.65% iR_f.

According to the strain data gathered from the LUNA OBR 4600, the SMPC OHS showed increasing strain behaviour with increasing temperature, even after compensating for the increasing strain due to the thermal expansion of the optical fibre sensor, aligning with the thermomechanical behaviour of the GTX SMPC. During the shape programming at 120°C and 140°C, the SMPC OHS showed a spring-back effect due to the instant elastic recovery. However, it showed 100% vR_f at 160°C with zero elastic recovery. At 160°C, the crosslinks of the SMP matrix fully enter their soft phase, enabling them to rearrange into the new shape. This can be primarily due to the crosslinks in the SMP network restricting the molecular mobility and incorporated GNP fillers suppressing the unwanted elastic recovery [25,26][27]. Once the heater was back to 160°C, the shape was recovered back (99.4%), showing the viscoelastic relaxation behaviour of SMPCs [28]. This can be clearly observed from the strain graphs at 120 and 140°C, with comparatively lower strains (Figure 12(a&b)) than the stains at 160°C (Figure 12(c)) in the exact sensor location with the 25 mm vertical deflection (Table 3). The change in the SMP matrix from the glassy phase to the rubbery phase at this temperature, allowing the SMPC component to achieve higher strains, can be mentioned as a reason for this behaviour. Therefore, maximum strain behaviour can be observed at 160°C temperature with the highest tensile strain of 1922.27±261.02 µStrain (Figure 12(c)). Interestingly, the stain graphs shown in Figure 4.12 indicate negative strain where the OHS underwent compression behaviour with a highest of -1940.38±292.38 µStrain at 160°C.

Table 3: Strain measurements of the SMPC OHS at different temperatures during 25 mm vertical deflection.

Average of 3 highest peaks	µStrain at 120°C	µStrain at 140°C	µStrain at 160°C

Maximum – Tensile Strain	602.71±98.08	658.78±160.40	1922.27±261.02
Minimum – Compression Strain	-819.85±63.33	-1018.75±198.11	-1940.38±292.38

The built-up resistance from the OHS can also be mentioned as a reason for encountering a lower iR_f value. Therefore, SMPC components with lower sector angles might be able to resolve this issue. During the recovery, the component showed excellent strain recovery ratios of 95.76% and 97.80% in the maximum tensile strain and compression strain measuring points, respectively. Furthermore, the SMPC OHS shows its increasing viscoelastic behaviour from the slowing recovery at different temperatures (Figure 12(d)). Showing the elastic behaviour at temperatures less than the T_s (131.68±1.79°C) value, the SMPC component showed lower recovered strain values (max: 91.96±15.89 and min: -125.54±12.44 µStrain) closer to zero strain at 120°C. However, the strain behaviour of the OHS at 160°C shows relatively closer recovered strain values (max: 220.16±12.73 and min: -143.90±151.22 µStrain) to the values mentioned above, even after a higher strain (max: 1922.25±261.01 and min: -1940.38±292.38 µStrain). Evidently, this is due to the shape memory effect related to the viscoelastic behaviour of the SMPC in action at increasing temperatures. Additionally, increased error margins of the measured strains can be due to the abnormal peaks that occur due to the anomalies in the composite, such as micro-cracks in the matrix [29].

The design of complex deployable shapes for space or lunar structures is still a grey area and needs a well-developed validation process to avoid critical failures. A reliable strain recovery method, such as DOFN has the ability to measure the deployability (shape fixity and recovery) of prototype SMPC structures, leading to the development of structures with optimal shapes.

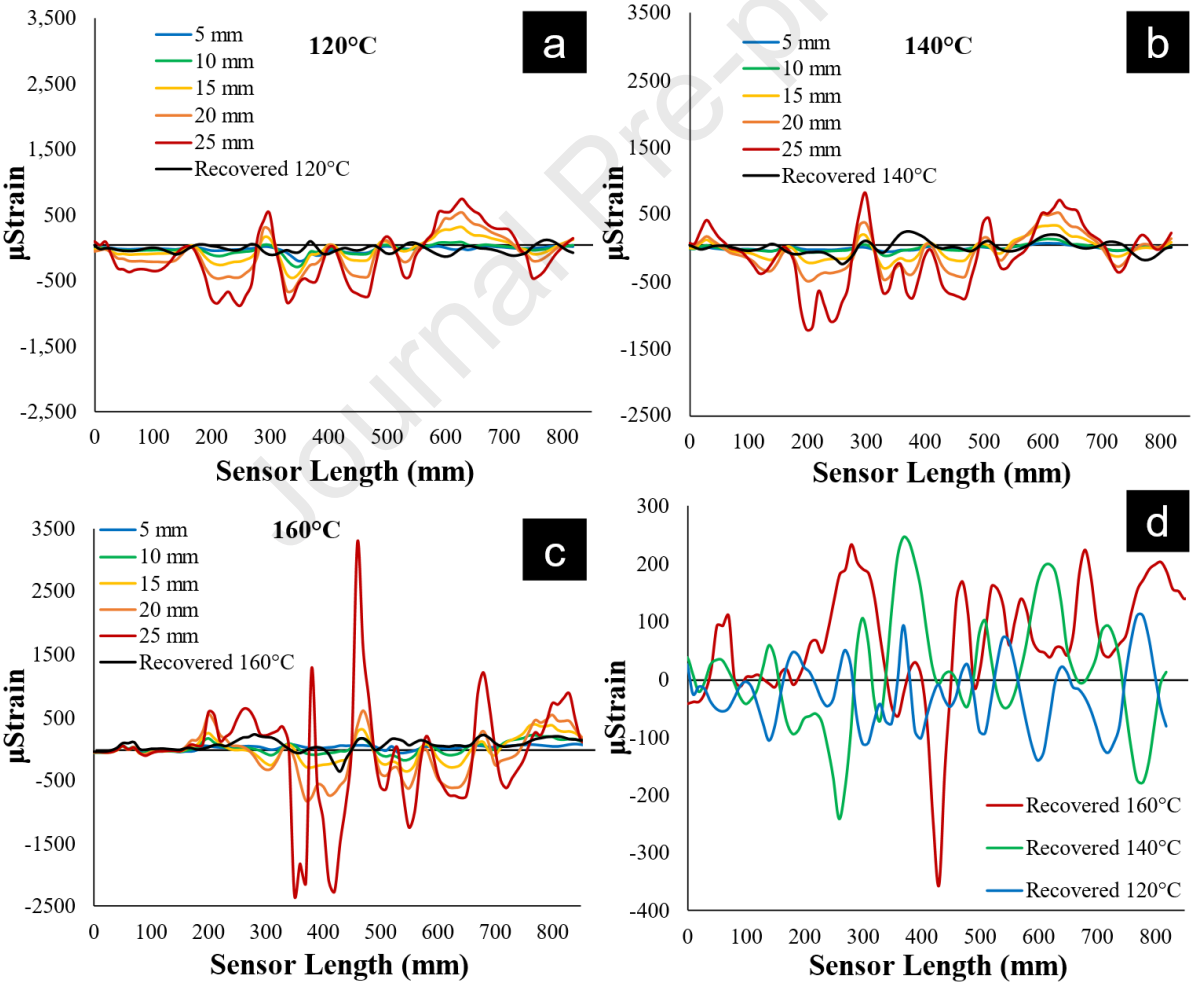

Figure 12: Strain behaviour of the SMPC OHS component at (a)120°C, (b)140°C, (c)160°C, and (d) the recovered strain at each mentioned temperature.

3.2 Bond strength analysis

The final hemispherical section was assembled using BACE adhesive layers and cured to reach maximum strength. The final assembly method of an actual structure on the moon can be based on either mechanical or

adhesive methods. However, this method can be further developed to match the actual construction techniques. The use of advanced adhesive application techniques and lowering the curing temperatures can make the assembly on the moon more practical. Furthermore, matching the thermal expansion coefficient of the SMPC and the adhesive material can be considered an added advantage. During the bond strength test, the adhesive bond joint of the SMPC failed due to a cohesive failure of the adhesive [30]. The tested samples showed an average bond strength of 64.86±2.79 MPa and a maximum traction separation load of 1.95±0.09 kN (Figure 13). Since the cured adhesive is high-temperature resistant BACE (up to ~250°C), the bond strength can be kept stable even at 130°C.

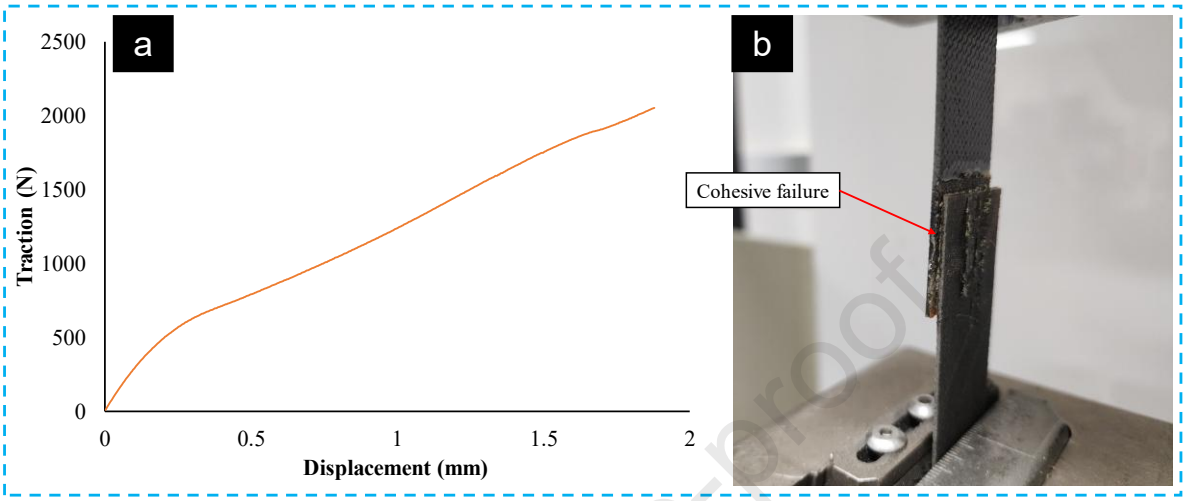

Figure 13: (a) Bond strength behaviour of the GTX SMPC and (b) Cohesive failure of the adhesive bond.

3.3 Finite Element Modelling

3.3.1 Finite element analysis – Validation of Shape Programming and Recovery of the SMPC Component

The SMPC OHS model was kept between two rigid blocks (one stationary and one moving) for the shape programming simulation. During Steps 1, 2, 3, 4, and 5, moving compression-head were given 5, 10, 15, 20, and 25 mm vertical deflections (displacements) to simulate the experimental shape programming steps (Figure A2 in Appendix). The final step allowed the component to recover by removing the total displacement.

During this simulation, the iR_f values of the developed FEA model were also validated, aligning with the experimental behaviour. The OHS FEA model (Figure 14) showed a 38.76% iR_f value, closer to the experimental iR_f value (42.54%). The possibility of a higher iR_f ratio of an SMPC component with smaller sectional angles was simulated using a half/hemi OHS (HOHS) with a 22.5° sectional angle, as shown in Figure 15. The new HOHS model, with a 45 mm maximum deflection (h_2) and an initial height (d_1) of 60 mm, achieved an iR_f value of 75%. This value can be important for large-scale components as it saves more space inside payloads.

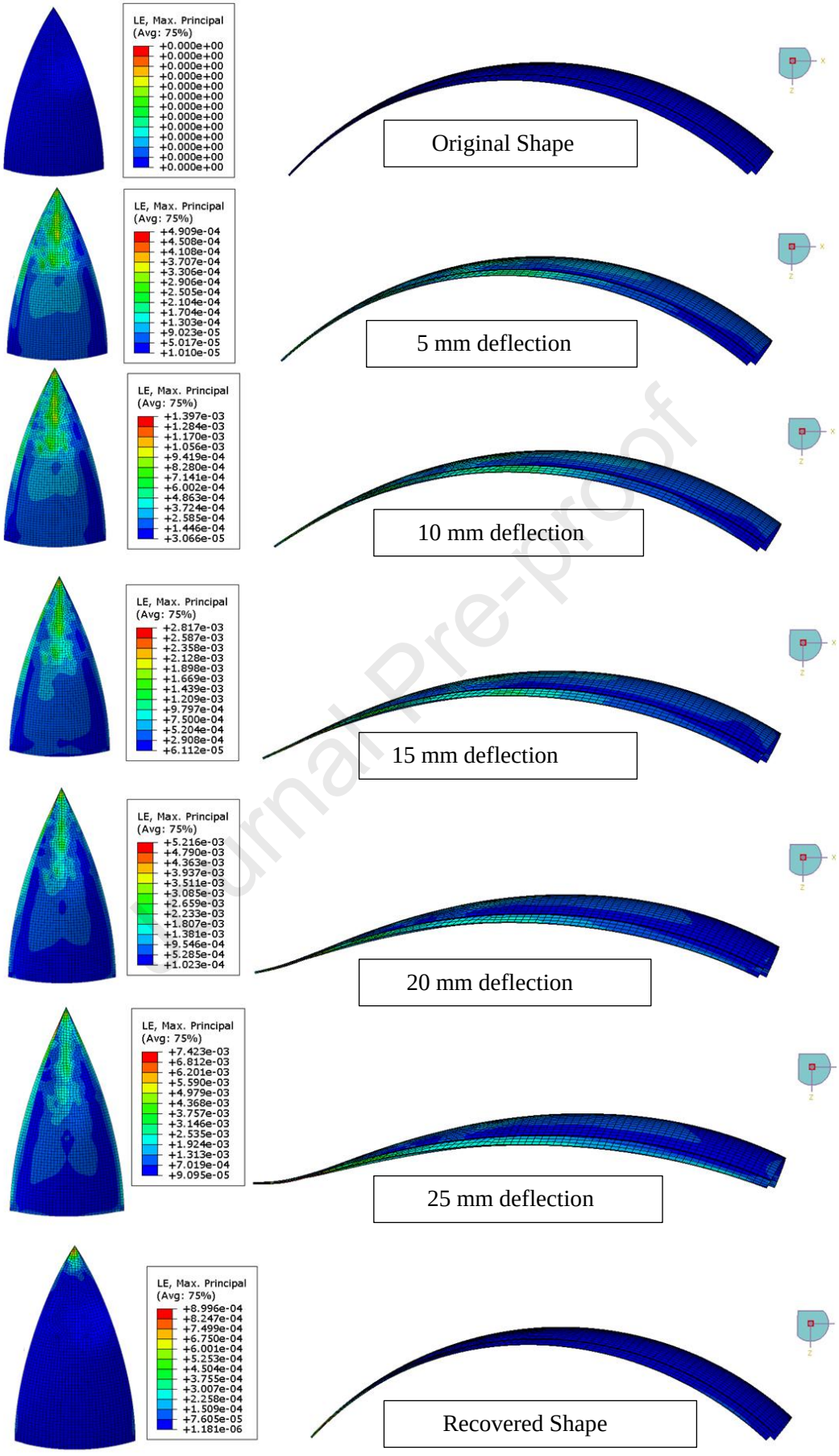

Figure 14: Shape fixity and recovery behaviour of the OHS FEA model- Plan view and Right View.

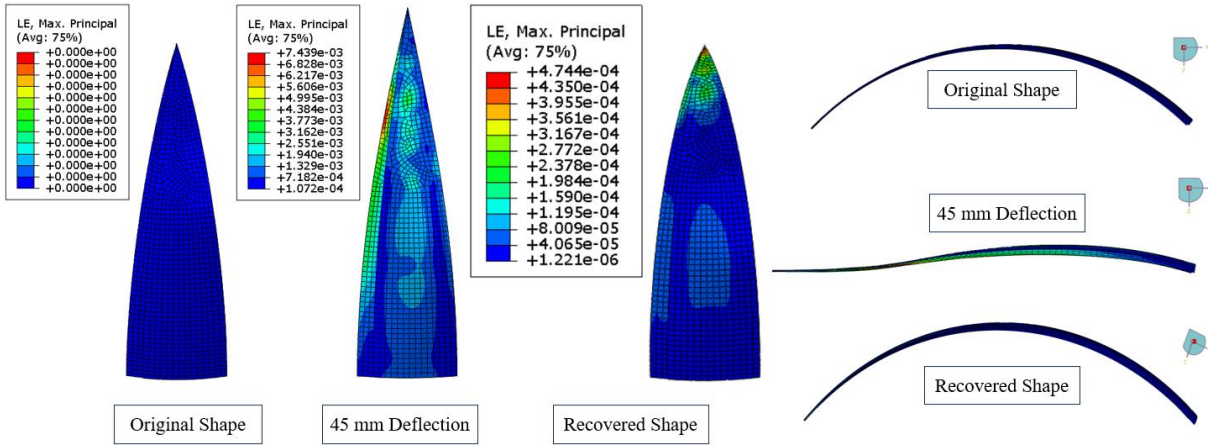

Figure 15: Shape programming and recovery of the SMPC Half-OHS component with a 22.5° sectional angle – Plan view (left), Right view (right).

Apart from the vertical shape fixity evaluation, measuring and validating the 3D shape fixity and recovery behaviour is important for the complex SMPC shapes. Therefore, measured µStrain values of designated measuring points were extracted from the strain graph in Figure 12(c) and shown in Figure 16. All the strain data was extracted after applying the user-specified spherical coordinate system to all elements and node-based results under the "Transformation" tool in the result section of ABAQUS. The graph shows the tensile and compression strains from points 1 to 11. Measuring points 3, 4, and 5 in the hoop direction showed the maximum strain compared to the strain readings in the axial direction.

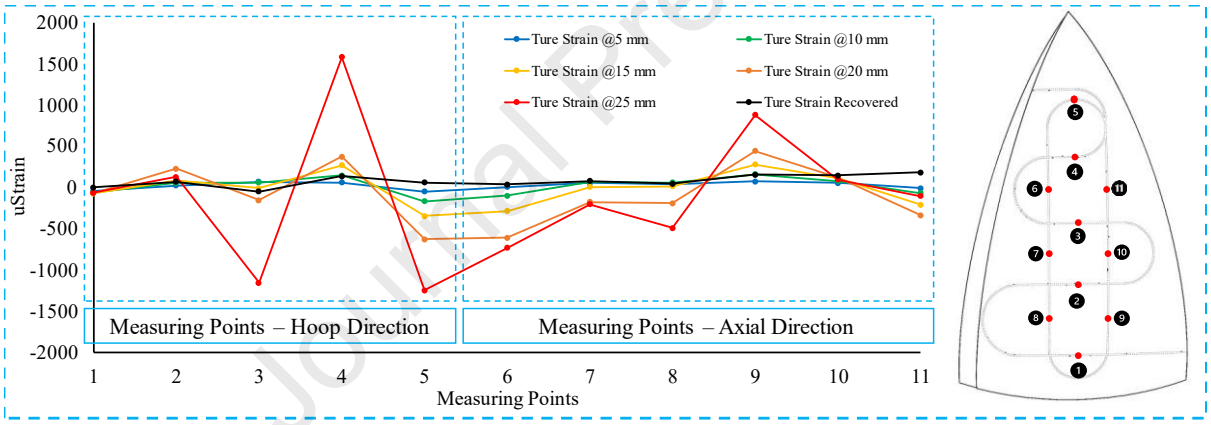

Figure 16: Measured µstrain values (at 160°C) at each designated point along the optical fibre sensor.

Aligning with the experimental optical fibre sensor lay-up, the strain measurement points (elements) in the FEA models were designated, as shown in the Appendix (Figure A3). Furthermore, the maximum absolute values were extracted for the tensile and compression strains using Max. Principal and Min. Principal strains, respectively. Extracted strain data from the FEA models were graphed against the experimental (True Strain) data of the SMPC component, as shown in Figure 17 and Figure 18. According to the figures, both OHS and half-OHS FEA models align with the strain behaviour of true strain data of the SMPC component. Furthermore, the half-OHS FEA model showed higher strain behaviour upon 45 mm vertical deflection. The R_r was calculated using the strain recovery behaviour shown in Table 4 achieved more than 95% recovery in all SMPC components and FEA models, validating the FEA models.

Table 4: Ideal shape fixity and recovery of SMPC component and FEA models.

Ideal shape fixity and Recovery at 160°C	**SMPC OHS**	**OHS FEA model**	**Half-OHS FEA model**
iR_f	42.54%	38.76%	75%
R_r (at max tensile strain point)	95.76%	98.23%	99.16%
R_r (at max compression strain point)	97.80%	98.87%	97.29%

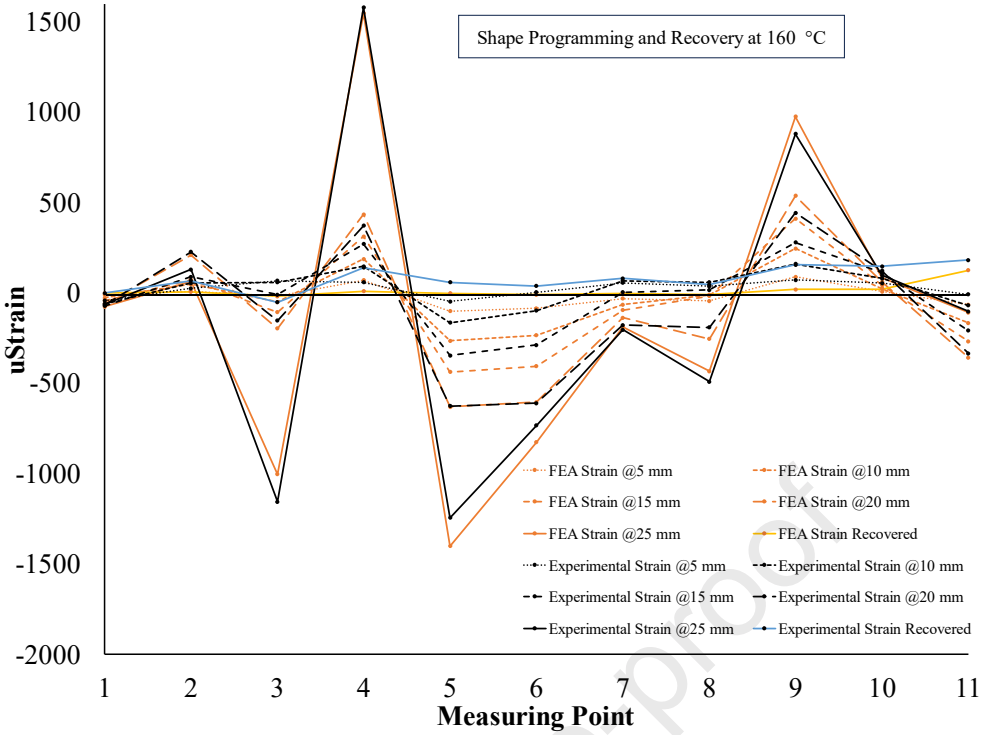

Figure 17: True strain behaviour of SMPC component and simulated strain behaviour of the OHS FEA model at 160°C.

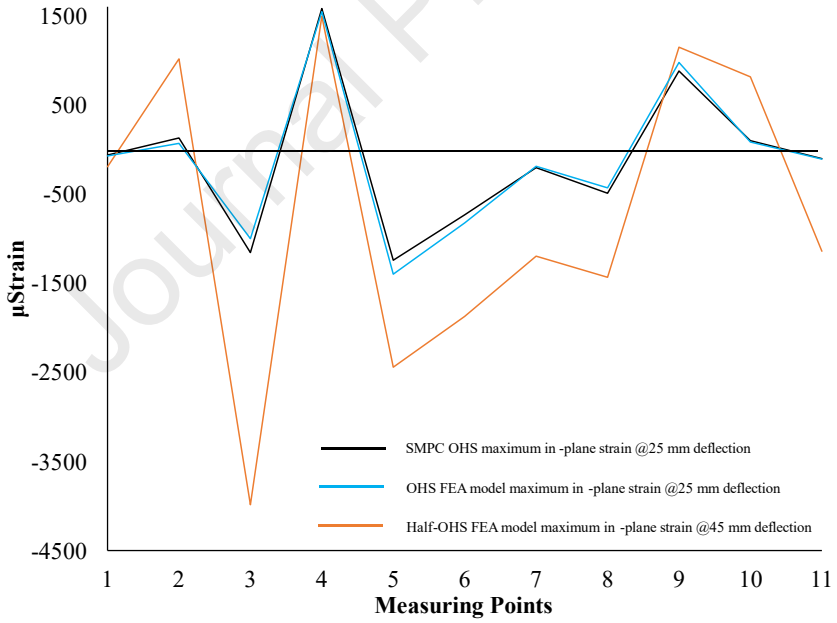

Figure 18: Strain behaviour of SMPC OHS, OHS FEA model, and Half-OHS FEA model under maximum vertical deflection.

Finally, the strain behaviour of the OHS under vertical displacement at 120°C was also validated (Figure 19). Although 120°C is a comparably higher temperature, it is considered in the range of maximum ambient temperature for the space and lunar environment. GTX SMPC component has shown a maximum of 504 µStrain tensile strain and 702.8 µStrain compressive strain upon the 25 mm vertical displacement, which is well below the failure strain of the GTX SMPC at 120°C. According to the validated FEA model, the maximum stress the model has gone through was 10.23 MPa, whereas the maximum stress of GTX SMPC at 120°C lies around ~67.44 MPa. Therefore, it is evident that the SMPC components can withstand additional stresses and strains at the lunar ambient temperature without failing. Additionally, these components might experience less stress in partial gravity on the moon or microgravity in space, extending their lifespan [31].

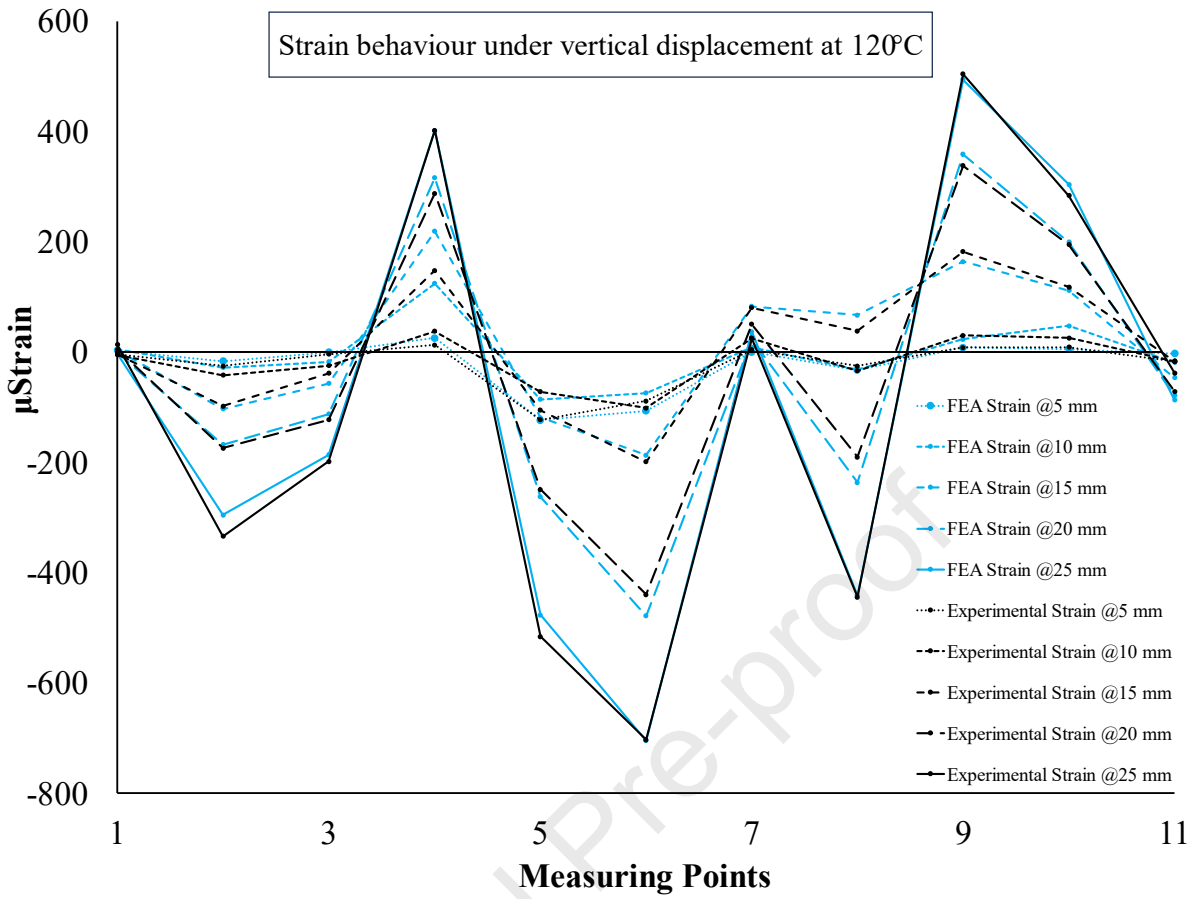

Figure 19: Strain behaviour of the OHS at 120°C compared to its FEA model.

The experimental OHS and its validated FEA model strengthen the claim of using SMPC structural components in rigid and deployable lunar habitats. In summary, SMPC components achieved over 95% experimental and over 98% simulated recovery ratios. According to the strain values from the FEA simulation, the SMPC OHSs have not exceeded their failure stress and strain values. The FEA-generated results show that the hemispherical sections with lower sectional angles can be programmed to achieve flat sheets without buckling them to be used as programmed components that can be stored, saving space and then recovered back in a vacuum environment.

3.3.2 Finite element analysis of the joint strength

As a necessary step for simulating the final assembled hemispherical thin-shell model, validating the bond strength of the single lap shear adhesive joint using the exact dimensions of the tested SMPC samples in a 2D planar modelling space, as shown in Figure 20. For the property definition, GTX SMPC was considered a quasi-isotropic material. As the main focus of this model, adhesive material was given the material properties of B9-N SMP (Table 2), which possess properties closer to those of the BACE pre-polymer adhesive. Since the adhesive materials showed a cohesive failure during the bond test, cohesive elements (Table 1) and properties were used according to the damage for traction separation laws.

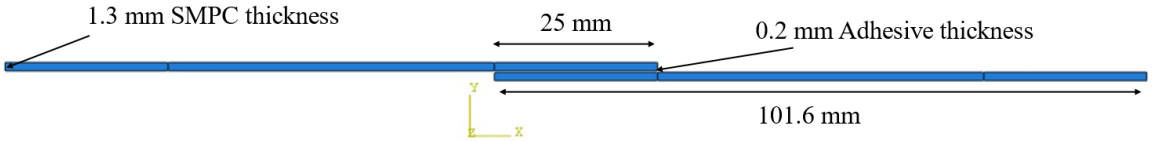

Figure 20: Dimensions of the single lap shear adhesive joint FEA model.

The model was given a 2 mm displacement during the simulation using the boundary conditions. At a strain of ~0.05, the adhesive layer started failing, as shown in Figure 21. The stress vs. strain behaviour was graphed along with the experimental adhesive joint strength behaviour, as shown in Figure 22. The experimental adhesive and FEA model showed similar behaviours, with closer maximum joint strengths of 64.87 MPa and 60.68 MPa,

respectively, validating the single lap-shear joined GTX SMPC. Therefore, using the properties of the B9-N SMP as the adhesive properties in the final hemispherical model will generate promising results.

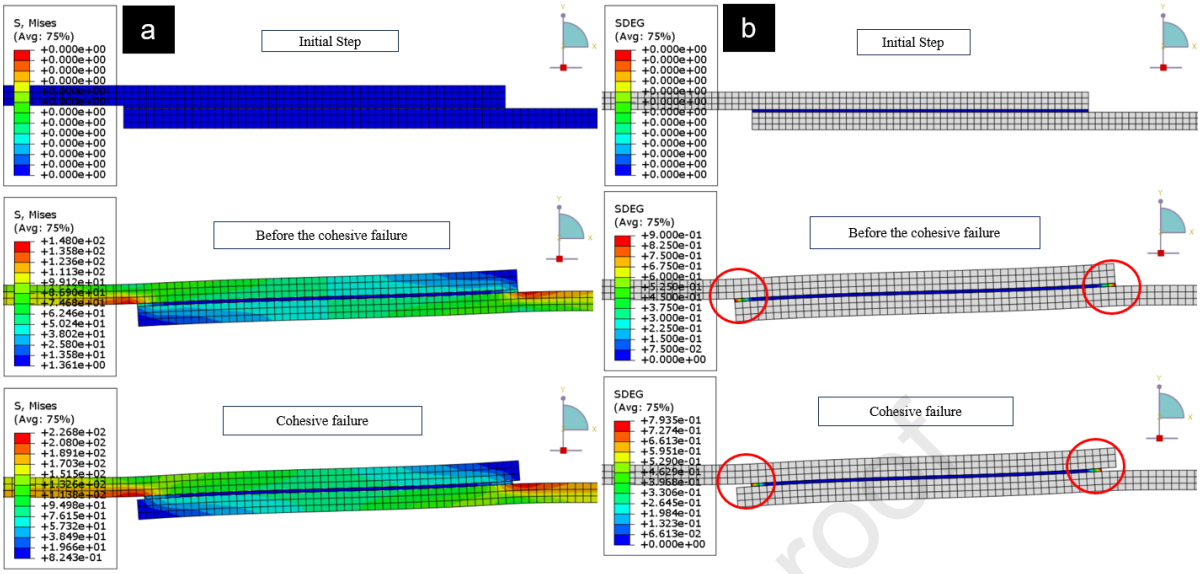

Figure 21: Cohesive failure of the joint in terms of (a) stress and (b) stiffness degradation.

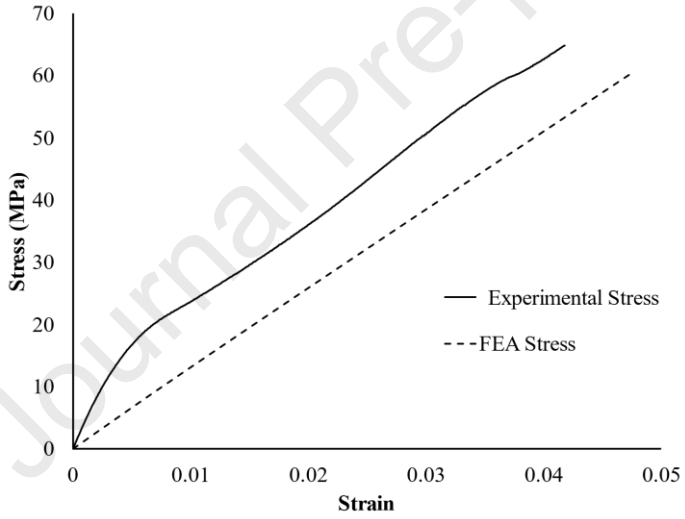

Figure 22: Stress vs Strain behaviour of the experimental and FEA single lap shear joined SMPCs.

3.3.3 Finite element analysis of the Dome under pressure

In the design and fabrication section of this study, GTX SMPC OHSs were assembled using the BACE adhesive, which is closer to the properties of BACE B9-N SMP. Once the hemispherical thin-shell dome is assembled, it is essential to check its performance under atmospheric pressure since it will be an individual dome or part of a hemispherical dish-ended pressure vessel-shaped habitat.

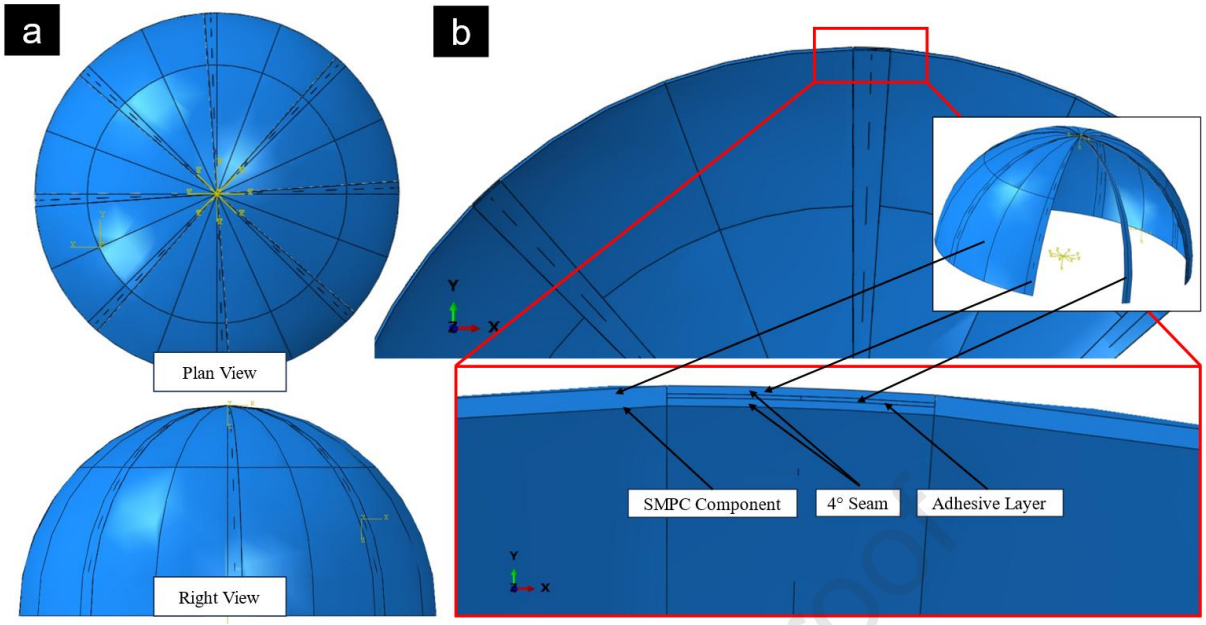

Figure 23: (a) Plan and Right view of the assembled hemispherical dome and (b) Assembled OHSs using the adhesive layer.

As shown in Figure 23, the OHSs and the adhesive layers were assembled to become a hemispherical section using the radial pattern tool in Abaqus. Then, all the adhesive surfaces were tied to the SMPC surfaces using the Surface to Surface Tie Constraint tool. Then, the outer rim of the hemispherical shape was fixed using the ENCASTRE option in boundary conditions. Then, 101325 Pa and 202650 Pa pressure loads were given inside the hemispherical section in two steps (Figure A4 in Appendix). An additional pressure of 202650 Pa (2 atm) was given to check the safety of the dome in increased pressure.

For the simulation, OHS was meshed using the Continuum Shell element type with Hex element shapes, as described in Table 1. However, the adhesive layer was meshed using the Cohesive element type with Wedge element shapes to avoid excessive distortion during the simulation. OHS and the adhesive layer consisted of 15909 elements and 221, respectively, for the considered FEA model in this section. Converging results with an error margin of ±5% were found in the same model with proper element refinement from 5169 to 10543 elements in the OHS model, and from 126 to 169 elements in the adhesive layer model. During the simulation, the air pressure did not affect a significant area in the model (Figure 24). However, the bottom side of the top section of the hemisphere and the adhesive layer were observed as the most stressed area, as shown in Figure 26. The stress values of three elements (3 points: point 1 from the top, point 2 from the middle and point 3 from the bottom) from three different areas of an OHS and the adhesive layers were extracted and graphed (Figure 25). The maximum stress the GTX SMPC component underwent was 127.55 MPa (GTX SMPC experimental max stress: 129.65±10.28 MPa) at 1 atm, and the adhesive layer underwent a maximum stress of 35.94 MPa (SMP adhesive experimental max stress: 64.86±2.79 MPa). Given the established convergence, the model is reliable for parametric studies, optimisation and performance evaluations, guaranteeing consistent and reproducible outcomes for future habitat applications. Since the spherical dome is aimed to withstand one atmospheric pressure, it can be highlighted that the FEA model confirmed that the SMPC dome can withstand it without failing [32]. Additionally, the overstressed areas of the FEA model can be used as a fail-safe dome structure. The main reason for this can be mentioned as the smaller area in the 4° seam to facilitate the given air pressure. However, this issue can be mitigated by redesigning the top section. Increasing the seam area, removing a part of the top section, adding a reinforced entrance, a modular connection point, or a window can be mentioned as a few remedies.

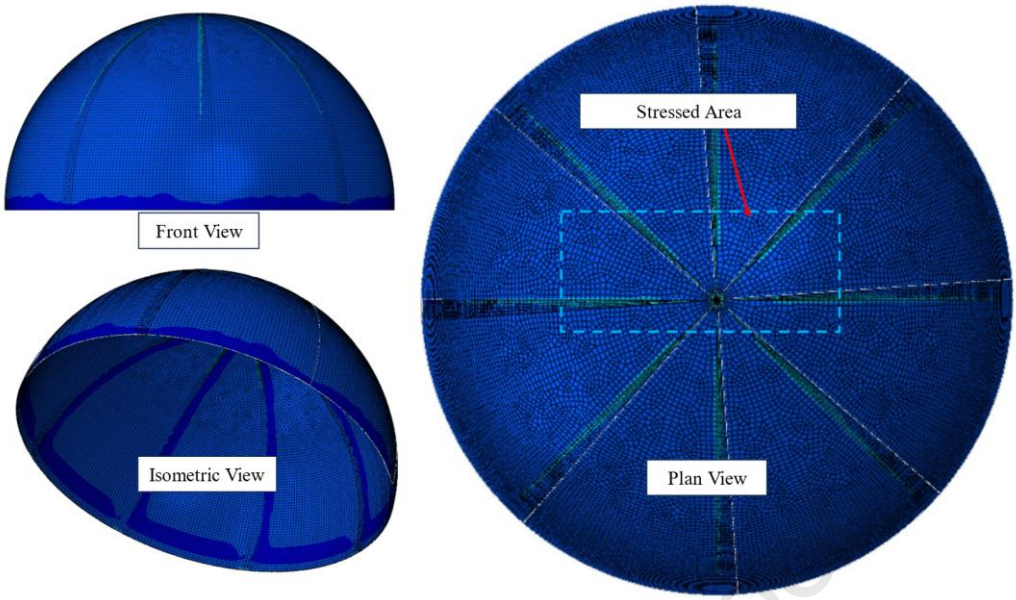

Figure 24: Meshed view of the assembled hemispherical dome FEA model and the maximum stress area of the model.

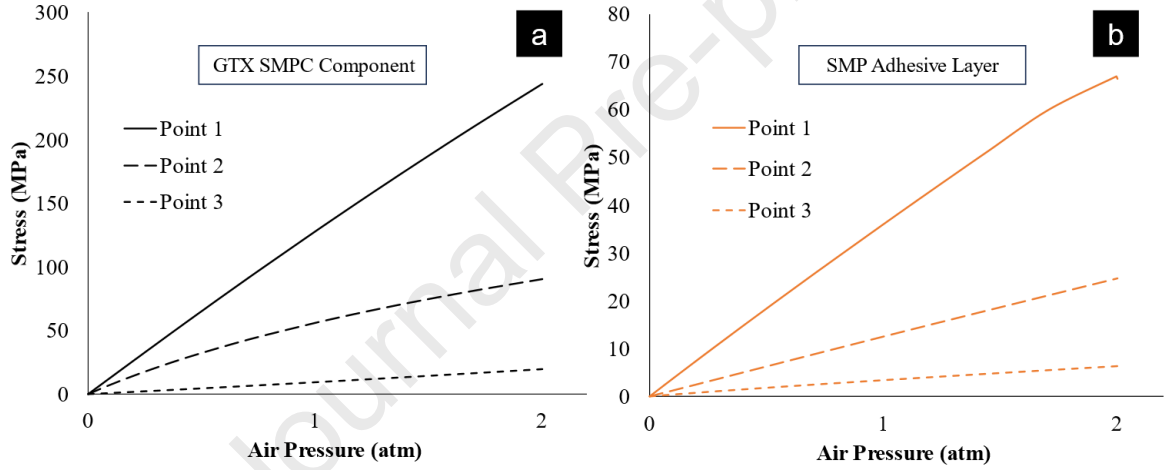

Figure 25: Stresses generated on the (a) GTX SMPC OHSs and (b) the SMP adhesive layer by different air pressures on the hemispherical section.

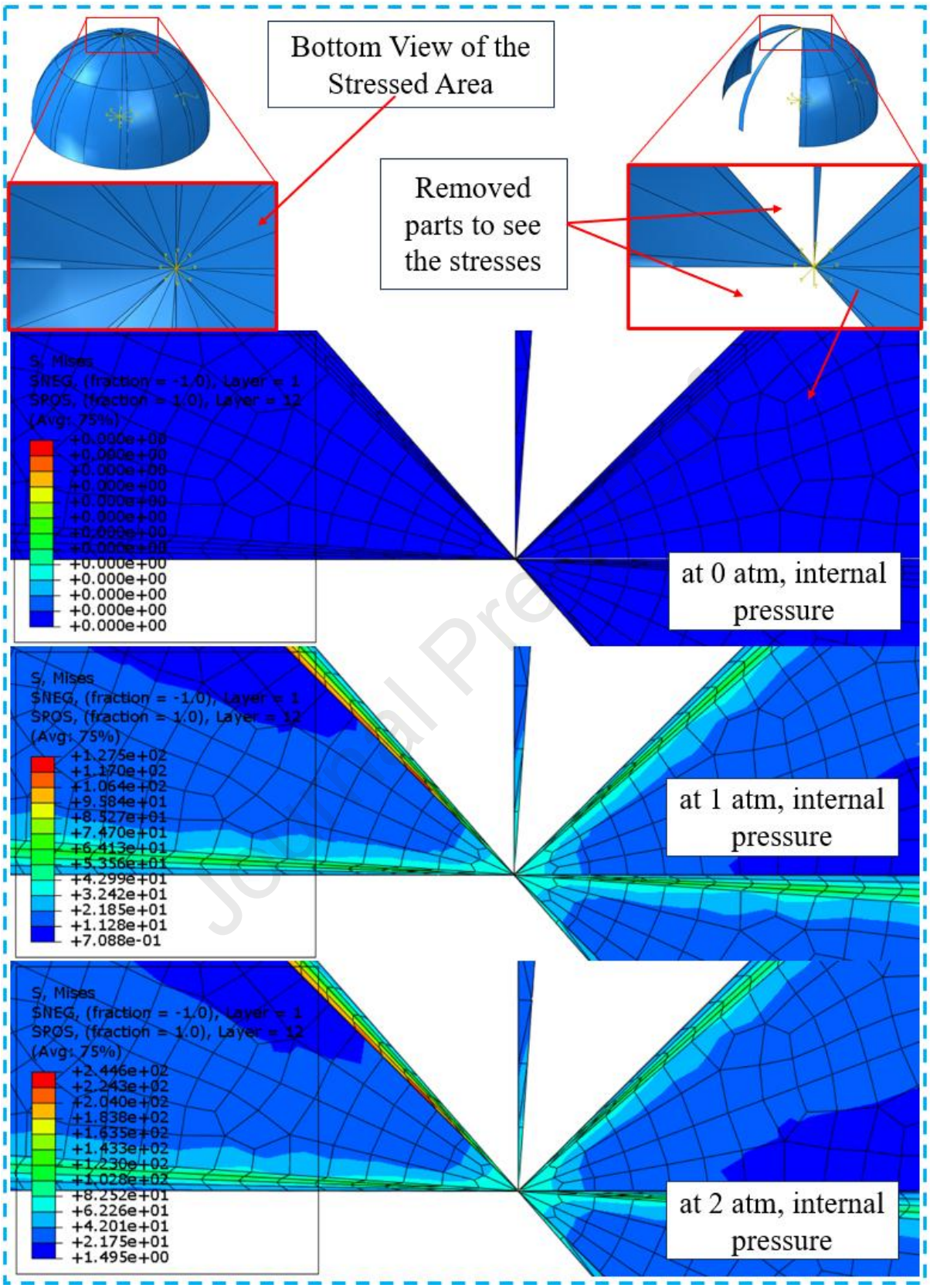

Figure 26: Stress behaviour of the assembled hemispherical dome model at 1 atm and 2 atm.

4 Conclusion

This study describes the manufacturing process and experimental and FEA validation of the fabricated OHSs and thin-shell hemispherical dome aimed at lunar habitation. A BACE and PEG-based SMP was synthesised using

a 9:1 stoichiometric ratio of BACE to PEG600, addressing the extreme temperatures in lunar and LEO environments. The SMP was reinforced and modified with glass fibres and GNP to achieve quasi-isotropic properties and efficient shape recovery. The 3D model of the OHS was designed for use in mould design and the FEA model. The developed SMP mixture and the GTX fibre lay-up architecture were used to fabricate the SMPC components. Finally, eight GTX SMPC OHSs were fabricated and assembled using BACE pre-polymer adhesive as the proof of concept. The fabricated components also underwent shape programming and recovery, showing a 42.54% ideal fixity ratio (iR_f) and 99.4% vertical recovery (vR_r) value. The micro-strain data from the DOFN showed excellent strain recovery ratios, with values above 95%. The simulated results aligned with a closer iR_f value of 38.54% and strain recovery values. The half-OHS FEA model proved that hemispherical sections with lower sectional values could increase the iR_f closer to 100% vertical shape fixity. It can be identified as a suitable method to flatten curved SMPC structural components to save storage space during transportation. The FEA model of the assembled SMPC dome structure was simulated under lunar habitat conditions. It showed adequate mechanical integrity under maximum stress levels that can be withstood by the GTX SMPC and SMP adhesive material. Furthermore, improving the assembly process and designs for more scaled up dome shape and other application-based shapes can be mentioned as future work.

This performance establishes it as a promising candidate for use in thin-shell habitat construction. The SMPC thin-shell component can be manufactured on Earth and programmed in the form of flattened sheets, which can be efficiently bundled for storage in payloads, ultimately saving both cost and time. Once in space or on the Moon, these components can be deployed to construct desired habitats and structures.

Acknowledgement

This research was supported by the Australian Government Research Training Program. The authors would like to extend their gratitude to Ms. Zaneta Senselova (PhD Candidate, UniSQ), Dr Hizam Rusmi (Senior Research Technical Officer), Dr Mazhar Peerzada (Senior Research Technical Officer), Mr Oliver Kinder (Senior Technical Officer), Mr Nathan Strenzel (Technical Officer), Mr. Graham Holmes (Technical Officer) and Mr. Brett Richards (Technical Officer) at the University of Southern Queensland, for their valuable assistance in this research.

References

[1] C. Heinicke, M. Arnhof, A review of existing analog habitats and lessons for future lunar and Martian habitats, Reach. 21–22 (2021) 100038. https://doi.org/10.1016/j.reach.2021.100038.

[2] M. Higgins, H. Benaroya, Utilizing the Analytical Hierarchy Process to determine the optimal lunar habitat configuration, Acta Astronaut. 173 (2020) 145–154. https://doi.org/10.1016/j.actaastro.2020.04.012.

[3] Q. Wang, P. Feng, K. Jansen, C. Bao, A novel rigidizable inflatable lunar habitation system: design concept and material characterization, Mater. Des. 246 (2024) 113289. https://doi.org/10.1016/j.matdes.2024.113289.

[4] C. Zeng, L. Liu, Y. Du, M. Yu, X. Xin, P. Xu, F. Li, L. Wang, F. Zhang, Y. Liu, J. Leng, Space-deployable device based on shape memory cyanate ester composites, Compos. Commun. 42 (2023) 101690. https://doi.org/10.1016/j.coco.2023.101690.

[5] F. Xie, X. Gong, L. Huang, L. Liu, J. Leng, Y. Liu, Effects of accelerated aging on thermal, mechanical, and shape memory properties of a cyanate-based shape memory polymer: II atomic oxygen, Polym. Degrad. Stab. 186 (2021) 109515. https://doi.org/10.1016/j.polymdegradstab.2021.109515.

[6] H. Gao, F. Xie, Y. Liu, J. Leng, Effects of γ-radiation on the performances of optically transparent shape memory polyimides with a low glass transition temperature, Polym. Degrad. Stab. 156 (2018) 245–251. https://doi.org/10.1016/j.polymdegradstab.2018.09.014.

[7] L. Luo, F. Zhang, L. Wang, Y. Liu, J. Leng, Recent Advances in Shape Memory Polymers: Multifunctional Materials, Multiscale Structures, and Applications, Adv. Funct. Mater. 34 (2024) 1–32. https://doi.org/10.1002/adfm.202312036.

[8] C. Zeng, L. Liu, Y. Du, M. Yu, X. Xin, P. Xu, F. Li, L. Wang, F. Zhang, Y. Liu, J. Leng, Space-deployable device based on shape memory cyanate ester composites, Compos. Commun. 42 (2023) 101690. https://doi.org/10.1016/j.coco.2023.101690.

[9] V.L. Le, V.T. Le, N.S. Goo, Deployment performance of shape memory polymer composite hinges at low temperature, J. Intell. Mater. Syst. Struct. 30 (2019) 2625–2638. https://doi.org/10.1177/1045389X19873403.

[10] Y. Liu, H. Du, L. Liu, J. Leng, Shape memory polymers and their composites in aerospace applications: A review, Smart Mater. Struct. 23 (2014). https://doi.org/10.1088/0964-1726/23/2/023001.

[11] F.F. Li, Y.J. Liu, J.S. Leng, Progress of Shape Memory Polymers and Their Composites in Aerospace Applications, Yuhang Xuebao/Journal Astronaut. 41 (2020) 697–706. https://doi.org/10.3873/j.issn.1000-1328.2020.06.007.

[12] X. Lan, L.W. Liu, F.H. Zhang, Z.X. Liu, L.L. Wang, Q.F. Li, F. Peng, S. Da Hao, W.X. Dai, X. Wan, Y. Tang, M. Wang, Y.Y. Hao, Y. Yang, C. Yang, Y.J. Liu, J.S. Leng, World's first spaceflight on-orbit demonstration of a flexible solar array system based on shape memory polymer composites, Sci. China Technol. Sci. 63 (2020) 1436–1451. https://doi.org/10.1007/s11431-020-1681-0.

[13] S. Jayalath, J. Epaarachchi, M. Herath, Lay-up configuration of glass fibre on cyanate ester based shape memory polymer composites, 11th Australas. Congr. Appl. Mech. (2024).

[14] S. Jayalath, M. Herath, J. Epaarachchi, E. Trifoni, E.E. Gdoutos, B. Samarasekara, Cyanate ester and polyethylene glycol based high temperature resistant shape memory polymer development for space applications, React. Funct. Polym. 201 (2024) 105949. https://doi.org/10.1016/j.reactfunctpolym.2024.105949.

[15] O.S. Ahmed, A. Aabid, J.S. Mohamed Ali, M. Hrairi, N.M. Yatim, Progresses and Challenges of Composite Laminates in Thin-Walled Structures: A Systematic Review, ACS Omega. 8 (2023) 30824–30837. https://doi.org/10.1021/acsomega.3c03695.

[16] S. Jayalath, E. Trifoni, J. Epaarachchi, M. Herath, E.E. Gdoutos, B. Samarasekara, Effect of atomic oxygen and vacuum thermal aging on graphene and glass fibre reinforced cyanate ester-based shape memory polymer composite for deployable thin wall

structures, Compos. Sci. Technol. 258 (2024) 110870. https://doi.org/10.1016/j.compscitech.2024.110870.
[17] M. Herath, C. Emmanuel, J. Jeewantha, J. Epaarachchi, J. Leng, Distributed sensing based real-time process monitoring of shape memory polymer components, J. Appl. Polym. Sci. 139 (2022). https://doi.org/10.1002/app.52247.
[18] J. Jeewantha, S. Jayalath, C. Emmanuel, Shape memory polymer smart plaster for orthopaedic treatments, (n.d.) 1–16.
[19] D.B. and B. Yang, A finite element model of shape memory polymer composite beams for space applications, Int. J. Numer. Methods Eng. (2015) 1102–1119. https://doi.org/10.1002/nme.4915nme.
[20] L.F.M. da Silva, R.J.C. Carbas, G.W. Critchlow, M.A.V. Figueiredo, K. Brown, Effect of material, geometry, surface treatment and environment on the shear strength of single lap joints, Int. J. Adhes. Adhes. 29 (2009) 621–632. https://doi.org/10.1016/j.ijadhadh.2009.02.012.
[21] L.D.C. Ramalho, R.D.S.G. Campilho, J. Belinha, L.F.M. da Silva, Static strength prediction of adhesive joints: A review, Int. J. Adhes. Adhes. 96 (2020) 102451. https://doi.org/10.1016/j.ijadhadh.2019.102451.
[22] N. Stein, J. Felger, W. Becker, Analytical models for functionally graded adhesive single lap joints: A comparative study, Int. J. Adhes. Adhes. 76 (2017) 70–82. https://doi.org/10.1016/j.ijadhadh.2017.02.001.
[23] G.D. Galletly, D.N. Moreton, A. Muc, Buckling of Slightly Flattened Domed Ends Reinforced Locally with Fibre-Reinforced Plastic, Proc. Inst. Mech. Eng. Part E J. Process Mech. Eng. 204 (1990) 15–24. https://doi.org/10.1243/PIME_PROC_1990_204_161_02.
[24] A. Muc, M. Chwał, M. Barski, Remarks on experimental and theoretical investigations of buckling loads for laminated plated and shell structures, Compos. Struct. 203 (2018) 861–874. https://doi.org/10.1016/j.compstruct.2018.07.094.
[25] R. Sanaka, S.K. Sahu, P.S.R. Sreekanth, K. Senthilkumar, N.D. Badgayan, B.V. Siva, Q. Ma, A Review of the Current State of Research and Future Prospectives on Stimulus-Responsive Shape Memory Polymer Composite and Its Blends, J. Compos. Sci. 8 (2024). https://doi.org/10.3390/jcs8080324.
[26] M. Lei, Z. Chen, H. Lu, K. Yu, Recent progress in shape memory polymer composites: Methods, properties, applications and prospects, Nanotechnol. Rev. 8 (2019) 327–351. https://doi.org/10.1515/ntrev-2019-0031.
[27] D. Bhattacharyya, Composite sheet forming, Elsevier, 1997. https://doi.org/https://www.google.com.au/books/edition/Composite_Sheet_Forming/Vv3DIQ0qDawC?hl=en&gbpv=0.
[28] K.D.C. Emmanuel, L.H.J. Jeewantha, H.M.C.M. Herath, J.A. Epaarachchi, T. Aravinthan, Shape memory polymer composite circular and square hollow members for deployable structures, Compos. Part A Appl. Sci. Manuf. 171 (2023) 107559. https://doi.org/10.1016/j.compositesa.2023.107559.
[29] B. Richter, L. Ulbrich, M. Herbers, S. Marx, Advances in Data Pre-Processing Methods for Distributed Fiber Optic Strain Sensing, Sensors. 24 (2024) 7454. https://doi.org/10.3390/s24237454.
[30] F.C. Campbell, Adhesive Bonding and Integrally Cocured Structure: A Way to Reduce Assembly Costs through Parts Integration, in: F.C.B.T.-M.P. for A.C. Campbell (Ed.), Manuf. Process. Adv. Compos., Elsevier, Amsterdam, 2004: pp. 241–301. https://doi.org/10.1016/B978-185617415-2/50009-5.
[31] P.M.G. Marquez, D. Smitherman, Common habitat design for microgravity, artificial gravity and partial gravity in a safe haven configuration, Accel. Sp. Commer. Explor. New Discov. Conf. ASCEND 2020. (2020). https://doi.org/10.2514/6.2020-4064.
[32] X. Liu, X.Y. Miao, S.S. Samareh-Mousavi, X. Chen, Finite element mesh transition for local–global modeling of composite structures, Compos. Part C Open Access. 15 (2024) 100510. https://doi.org/10.1016/j.jcomc.2024.100510.

Appendix

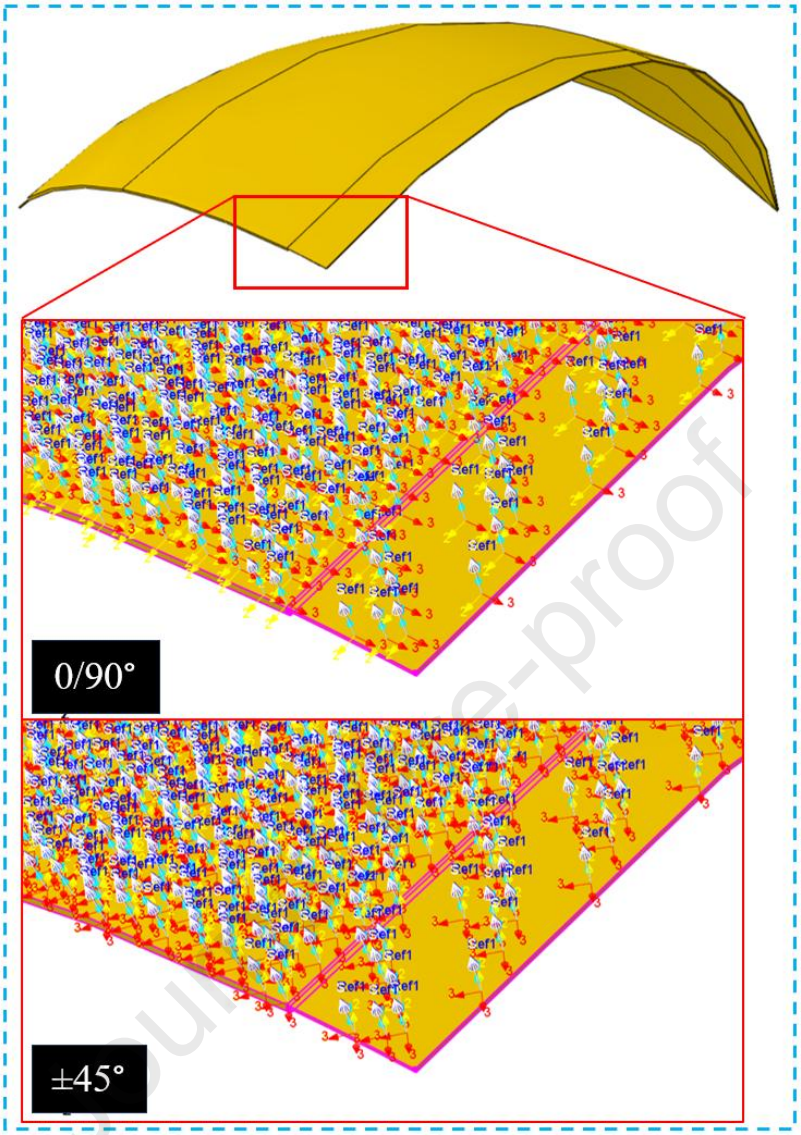

Figure A1: Fibre layup configurations of the FEA model.

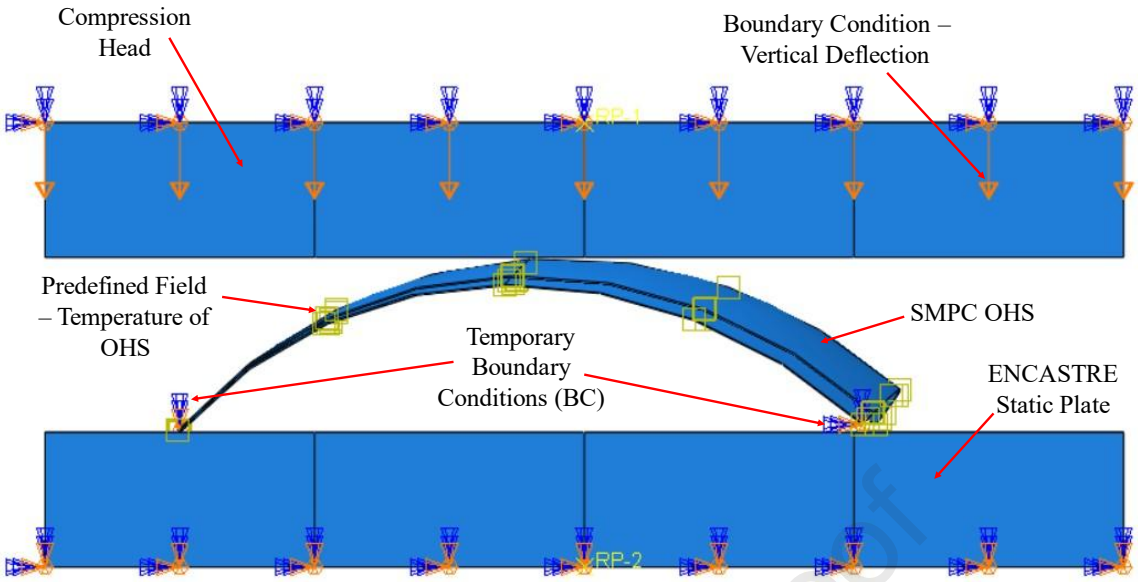

Figure A2: Vertical deflection and the boundary conditions of the OHS FEA model.

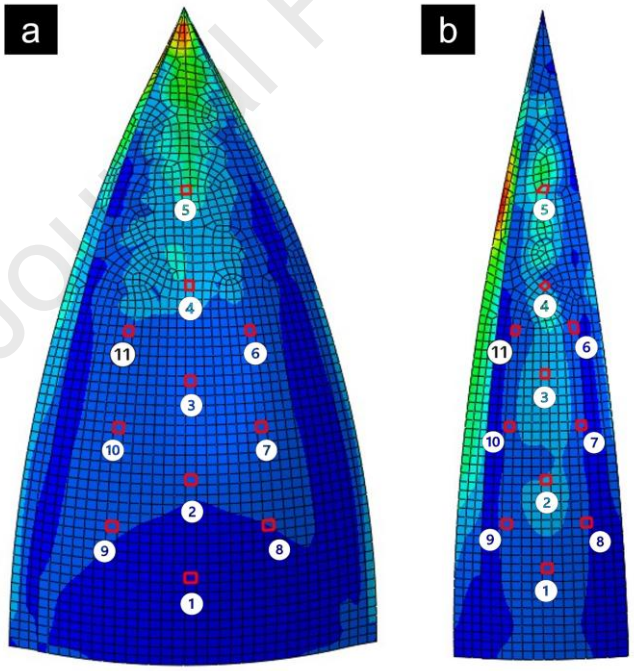

Figure A3: Strain measurement points in the (a) OHS FEA model and the (b) Half-OHS FEA model.

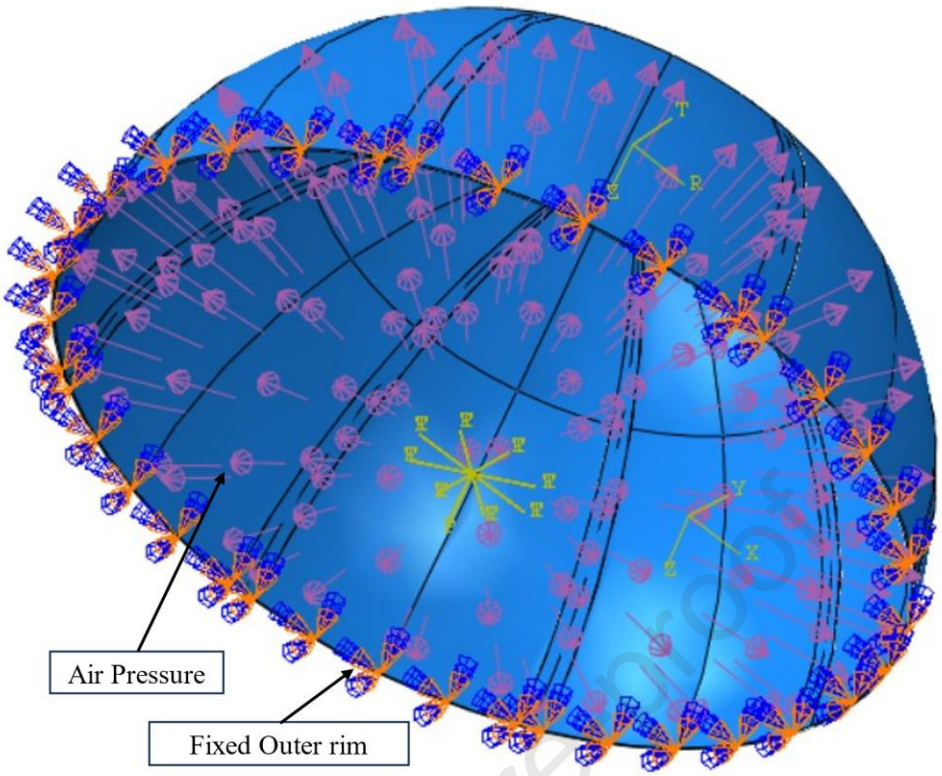

Figure A4: Pressurised hemispherical section.

Design and fabrication of lightweight thin-shell structures using shape memory polymer composites for lunar habitat systems

Sandaruwan Jayalath[a,b,c], Uditha Roshan[d], Janitha Jeewantha[a,b], Jayantha Epaarachchi[1,a,b], Eduardo Trifoni[e], Madhubhashitha Herath[a,f], Eleftherios E. Gdoutos[g,h], Bandu Samarasekara[i]

[a]*Centre for Future Materials & Institute of Advanced Engineering and Space Sciences, University of Southern Queensland, Toowoomba, QLD 4350, Australia.*
[b]*School of Engineering, Faculty of Health, Engineering and Sciences, University of Southern Queensland, Toowoomba, QLD 4350, Australia.*
[c]*Division of Polymer and Chemical Engineering Technology, Institute of Technology University of Moratuwa, Diyagama, Sri Lanka*
[d]*Queensland Micro and Nanotechnology Centre, Griffith University, Nathan, QLD 4111,Australia.*
[e]*School of Astronomy and Astrophysics, Australian National University, Canberra, Australia.*
[f]*School of Engineering, University of Hull, UK*
[g]*Graduate Aerospace Laboratories, California Institute of Technology, Pasadena, California, 91125, USA.*
[h]*Proteus Space, Inc., Los Angeles, CA 90021*
[i]*Department of Materials Science and Engineering, University of Moratuwa, Sri Lanka.*

Abstract

The increasing demand for lightweight, rigid, and deployable structures in space exploration has driven the development of advanced materials for lunar and orbital habitats. This study presents the design, fabrication, and validation of modular thin-shell components based on shape memory polymer composites (SMPCs) for deployable rigid habitats. Moreover, the durability in unexplored, harsh environmental conditions and the lower weight are the governing factors for these materials. In this context, well-developed and durable shape memory polymer-based composites (SMPCs) are ideal for these habitats due to their potential to create lightweight, thin-shell structures and their proven ability to revert to their original shape when stimulated by external factors, such as heat and light. Furthermore, this enables the manufacture of SMPC habitat components on Earth, allowing for reduced storage space in payloads, and facilitates the recovery and rebuilding of habitats after transportation. During this study Bisphenol-A cyanate ester based shape memory polymer was synthesised and reinforced with glass fibres and graphene nanoplatelets to achieve quasi-isotropic properties and enhanced thermal stability. Using vacuum-assisted resin infusion, hemispherical thin-shell modules (1 mm thickness) were manufactured and programmed into compact configurations for efficient payload storage. Experimental evaluation demonstrated excellent shape recovery (>95%) and adhesive joint strength, while distributed optical fibre sensing enabled precise strain mapping during programming and recovery. Finite element analysis validated the structural integrity of the assembled dome under internal pressures up to 2 atm, confirming its suitability for lunar habitat applications. Furthermore, this work can be considered one of the pioneering works to use space grade SMPCs in future lunar habitats. The proposed SMPC-based architecture offers a promising solution for lightweight, reconfigurable structures in future space missions, combining deployability, mechanical robustness, and thermal resilience.

Keywords: *Cyanate esters, deployable rigid structures, lunar habitats, shape memory polymer composites, space applications, thin-shell structures.*

[1] Corresponding author at: School of Engineering, Faculty of Health Engineering and Sciences, University of Southern Queensland, Toowoomba, 4350 QLD, Australia.
E-mail address: Jayantha.Epaarachchi@unisq.edu.au (J.A.Epaarachchi).

Declaration of interests

☒ The authors declare that they have no known competing financial interests or personal relationships that could have appeared to influence the work reported in this paper.

☐ The authors declare the following financial interests/personal relationships which may be considered as potential competing interests: